UNCLASSIFIED

AD **408 271**

DEFENSE DOCUMENTATION CENTER

FOR

SCIENTIFIC AND TECHNICAL INFORMATION

CAMERON STATION, ALEXANDRIA, VIRGINIA

UNCLASSIFIED

TRANSVERSE DOPPLER PATTERN MEASUREMENT TECHNIQUE

H. H. Hougardy
R. K. McFadden

Teledyne Systems Corporation
Electromagnetic Systems Division
Hawthorne, California

Final Report

1 February 1963

Prepared for

Electronic Research Directorate
Air Force Cambridge Research Laboratories
Office of Aerospace Research
United States Air Force
Bedford, Massachusetts

FOREWORD

The authors wish to acknowledge the technical assistance of Dr. R. W. Bickmore, and Messrs. H. E. Shanks and R. J. Spellmire in performing the analytic portion of the work contained in this report. The computer programming and associated computations were ably performed by Messrs. C. A. Bean and E. E. Stafford.

ABSTRACT

This report contains the results of an analytic investigation of the Transverse Doppler Pattern Measurement Technique for determining the far field radiation characteristics of large antennas from near field measurements. The technique is based on using Doppler signal processing to obtain the information necessary for predicting the far field patterns of large antennas in their site environments. Primary emphasis has been placed on establishing a rigorous mathematical description of the measurement process from which system parameters and performance may be determined.

Several mathematical models have been developed which differ both in the analytical approach and in the physical make-up of the measuring system. Mathematical approximations for the diffraction field of the aperture have been expanded in several coordinate frames. The signal processing systems investigated include multichannel processing, synthetic aperture processing, and directional and nondirectional sampling antennas. Attention has been given to linear arrays, rectangular arrays with separable and nonseparable distributions, circular apertures with circularly symmetric distribution, and arbitrarily shaped radiating apertures with large linear phase deviations. Two experimental procedures have been outlined for the purpose of verifying the feasibility of the analytical work.

CONTENTS

CONTENTS (Continued)

ILLUSTRATIONS

ILLUSTRATIONS (Continued)

I. INTRODUCTION

The far field behavior of antennas is customarily measured at distances which exceed or are at least equal to $2D^2/\lambda$, where D is the aperture diameter and λ is the operating wavelength in free space. For many large antennas, especially those used for radio astronomy, conventional methods of pattern measurement at this distance are always difficult and often impossible. For this reason, various other techniques have been utilized in obtaining desired data on the far field performance of these large antennas. These techniques include actual far field measurements using aircraft, balloons, and radio stars to obtain the required measurement distance as well as near field measurements such as probing the aperture field to obtain the aperture distribution and focusing the antenna within the near field.[1,2,3] Such techniques are, in general, straightforward extensions of conventional pattern measurement procedures and are more or less satisfactory depending on the particular antenna being evaluated. They are usually involved and time consuming and, in some cases, require modification of the antenna from its operational configuration with a resultant uncertainty in the measured data.

Described in this report is the analytic investigation of the application of Doppler techniques to the large antenna pattern measurement problem in an attempt to overcome the various difficulties associated with more conventional methods of measurement. The aperture distribution is obtained by processing the signal received by a probe antenna which moves at high velocity across the radiating aperture at a distance which is a small fraction of its far field distance. The far field radiation pattern is then obtained directly from the measured aperture distribution by performing the radiation integration. The analytic expressions

which form the basis of the Transverse Doppler Pattern Measurement Technique are considered in detail and various methods of signal processing are examined. The technique is applied to various antenna configurations and computations of the results are presented. Experiments for determining the feasibility of the measurement technique are also discussed.

II. GENERAL ANALYSIS

Under the assumption that the antenna whose characteristics are to be measured may be represented by an aperture lying in the ξ, η plane and that the aperture field is uniformly polarized in the ξ-direction, the diffraction field is given by (using Silver's scalar field approximation[4]):

$$U_p = \frac{\exp(j\omega_o t)}{4\pi} \int_A F(\xi, \eta) \frac{\exp(-jkr)}{r} \left[\left(jk + \frac{1}{r}\right)\hat{i}_z \cdot \hat{r}_1 + jk\hat{i}_z \cdot \hat{s}\right] d\xi d\eta \qquad ($$

for the geometry of Figure 1a. In the equation,

$F(\xi, \eta) = A(\xi, \eta) \exp\left[j\Psi(\xi, \eta)\right]$, the aperture distribution

$\hat{r}_1$ is a unit vector in the direction from the aperture point ξ, η to the field point P

$\hat{s}$ is a unit vector along a ray through the aperture.

Equation (1) may be considerably simplified under the following conditions:

i. $k >> \frac{1}{r}$ or $kr >> 1$

ii. $\hat{i}_z \cdot \hat{r}_1 \cong \hat{i}_z \cdot \hat{R}_1 = \cos\theta \cong 1$

iii. $\hat{i}_z \cdot \hat{s} \cong 1$

The first condition requires that the measurement distance be large compared with the operating wavelength. The second requires that the

3
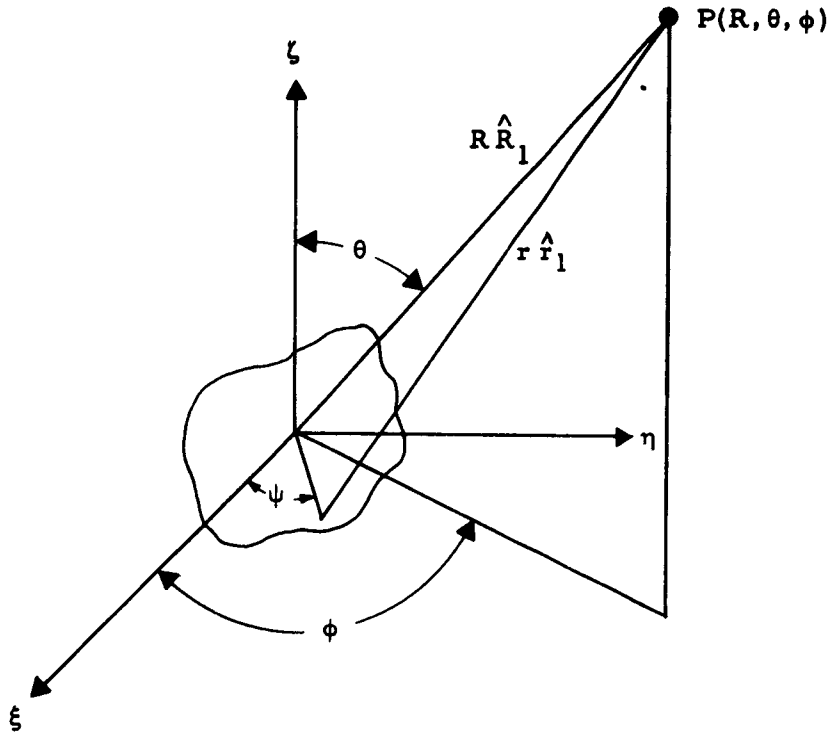
Figure 1a.   Geometry and Coordinate System
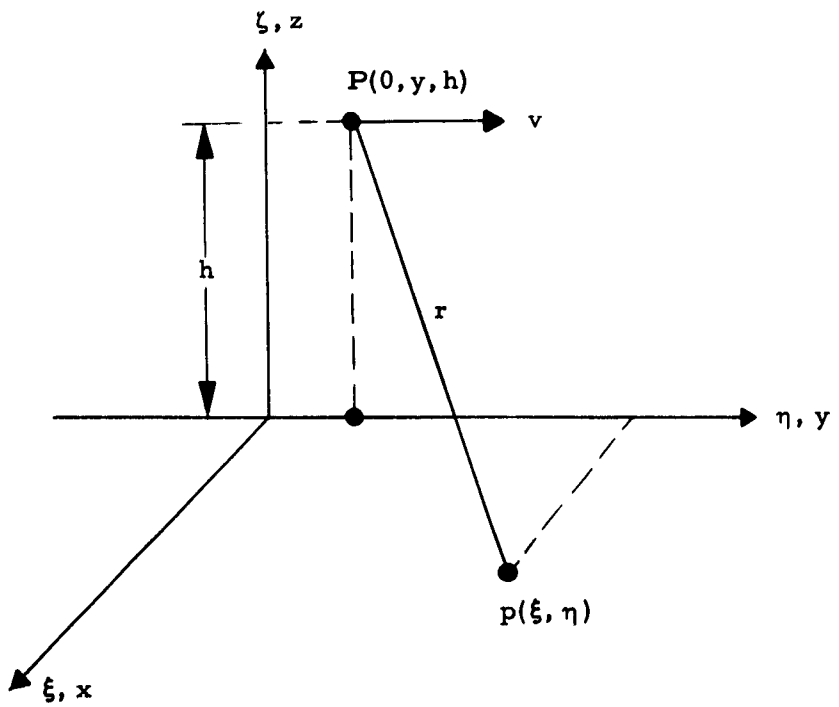
Figure 1b.   Aperture and Space Coordinate System

4

measurement distance be large enough so that the unit vector $\hat{r}_1$, directed from an arbitrarily located current element on the aperture to the field point P, is essentially parallel to the unit vector $\hat{R}_1$ directed from the center of the aperture to the field point, and that the antenna main beam be at or near broadside. The third condition requires that the phase distribution be essentially planar. These conditions are, in general, adequately met for large antennas of the type being considered here, and the scalar diffraction equation reduces to

$$U_p = \frac{jk \exp(j\omega_o t)}{2\pi} \int_A F(\xi, \eta) \frac{\exp(-jkr)}{r} \, d\xi d\eta \qquad (2)$$

Now assume that the diffraction field is sampled with an omnidirectional probe antenna which is moving across the aperture at a constant height h with a constant velocity v. The probe path is described by the space coordinates x = 0, y is variable, and z = h. The y-axis is coincident with the η-axis, and the origin of the space coordinate system coincides with that of the aperture coordinate system as indicated in Figure 1b.

In rectangular coordinates, r may be expressed as

$$r = \left[\xi^2 + (\eta - y)^2 + h^2 \right]^{1/2} \qquad (3)$$

Thus, in terms of the parameters, h and y, the radiated field along the probe path is

5

$$g_y(h, y) = \frac{jk \exp (j\omega_o t)}{2\pi} \int_{\eta_1}^{\eta_2} d\eta \int_{c_1(\eta)}^{c_2(\eta)} d\xi F(\xi, \eta)$$

$$\cdot \frac{\exp\left\{-jk\left[h^2 + \xi^2 + (y - \eta)^2\right]^{1/2}\right\}}{\left[h^2 + \xi^2 + (y - \eta)^2\right]^{1/2}} \quad . \tag{4}$$

For y a linear function of time (corresponding to a constant probe velocity)

$$y = vt \quad ; \quad -\infty \le t \le +\infty$$

and

$$g_y(h, vt) = \frac{jk \exp (j\omega_o t)}{2\pi} \int_{\eta_1}^{\eta_2} d\eta \int_{c_1(\eta)}^{c_2(\eta)} d\xi F(\xi, \eta)$$

$$\cdot \frac{\exp\left\{-jk\left[(vt - \eta)^2 + h^2 + \xi^2\right]^{1/2}\right\}}{\left[(vt - \eta)^2 + h^2 + \xi^2\right]^{1/2}} \quad . \tag{5}$$

Now let us consider the effect of passing this time dependent signal through a bandpass filter as it is received at the probe antenna. The spectral density of the signal after passage through the filter is found using the Fourier transform pair:

$$g(t) = \frac{1}{\sqrt{2\pi}} \int_{-\infty}^{\infty} G(\omega) \exp(j\omega t) \, d\omega$$

(6)

$$G(\omega) = \frac{1}{\sqrt{2\pi}} \int_{-\infty}^{\infty} g(t) \exp(-j\omega t) \, dt \quad .$$

For a filter with a characteristic function $H(\omega)$, the spectral density of the output signal is

$$S_y(\omega) = H(\omega) \, G(\omega)$$

(7)

and the output signal is (using Equation (6) above)

$$S_y(t) = \frac{1}{\sqrt{2\pi}} \int_{-\infty}^{\infty} S_y(\omega) \exp(j\omega t) \, d\omega$$

$$= \frac{j}{(2\pi)^2} \int_{\eta_1}^{\eta_2} d\eta \int_{c_1(\eta)}^{c_2(\eta)} d\xi F(\xi, \eta) \int_{-\infty}^{\infty} d\omega H(\omega) \exp(j\omega t)$$

$$\bullet \int_{-\infty}^{\infty} k \, \frac{\exp\left\{-jk\left[(vt' - \eta)^2 + h^2 + \xi^2\right]^{1/2}\right\}}{\left[(vt' - \eta)^2 + h^2 + \xi^2\right]^{1/2}} \, \exp\left[-j(\omega - \omega_o) t'\right] dt' \quad .$$

(8)

This equation is, in general, quite difficult to evaluate because of the complicated way in which both the space and time variables appear.

Some simplification of the mechanics of the integrals may be obtained by carefully choosing the filter characteristics

As examples, consider the filter functions

$$H_1(\omega) = \begin{cases} 1 & ; \quad \omega_o - \dfrac{B}{2} \leq \omega \leq \omega_o + \dfrac{B}{2} \\ \\ 0 & ; \quad \text{elsewhere} \end{cases}$$ (9

$$H_2(\omega) = \frac{\sin\left(\dfrac{\omega - \omega_o}{2B}\right)}{\omega - \omega_o}$$ (1(

where B is the filter bandwidth. For these cases Equation (8) may be integrated to give

$$S_{y_1}(t) = \frac{jk \exp(j\omega_o t)}{2\pi^2} \int_{\eta_1}^{\eta_2} d\eta \int_{c_1(\eta)}^{c_2(\eta)} d\xi F(\xi, \eta)$$

$$\bullet \int_{-\infty}^{\infty} \frac{\exp\left(-jk\left\{\left[v(t'' + t) - \eta\right]^2 + h^2 + \xi^2\right\}^{1/2}\right)}{\left\{\left[v(t'' + t) - \eta\right]^2 + h^2 + \xi^2\right\}^{1/2}} \frac{\sin \dfrac{B}{2} t''}{t''} \, dt''$$

for the flat top bandpass filter and

$$S_{y_2}(t) = \frac{jk \exp(j\omega_o t)}{4\pi} \int_{\eta_1}^{\eta_2} d\eta \int_{c_1(\eta)}^{c_2(\eta)} d\xi F(\xi, \eta)$$

$$\cdot \int_{-1/2B}^{1/2B} \frac{\exp\left(-jk\left\{\left[v(t''+t)-\eta\right]^2 + h^2 + \xi^2\right\}^{1/2}\right)}{\left\{\left[v(t''+t)-\eta\right]^2 + h^2 + \xi^2\right\}^{1/2}} dt'' \tag{12}$$

for the $\frac{\sin u}{u}$ filter. However, it appears that neither of these equations can be integrated further in closed form.

At this point it is advisable to consider the physical counterpart of the mathematical expression derived above. For a vehicle moving at a velocity v and a height h above a plane surface which is uniformly radiating energy at a frequency f_o, the frequency of the energy received at the vehicle from any point on the plane will be shifted from f_o by an amount proportional to the relative velocity with which the vehicle is approaching or receding from the radiating point. This is the well-known Doppler frequency relation. It may be readily shown that the points on the plane for which the received energy has a constant Doppler shift at any given instant form a family of hyperbolas with a straight line directly below the vehicle and transverse to its path as the limiting case corresponding to zero Doppler shift. Therefore, filtering at f_o allows passage of only those frequency components which correspond to signals radiated from the region between two hyperbolas on the plane surface as indicated in Figure 2a. This sampling region moves with the vehicle as it passes over the plane. If the portion of the plane which radiates is now constrained to be an antenna aperture, the effect is that of moving a sampling function progressively over the aperture as shown in Figure 2b.
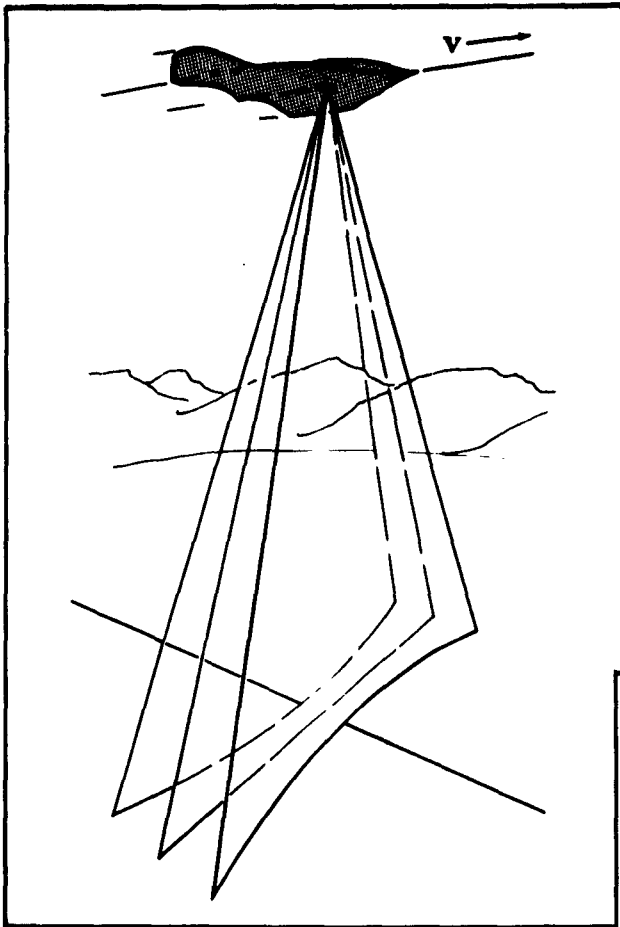
Figure 2a. Constant Doppler Frequency
Trace on Plane Surface
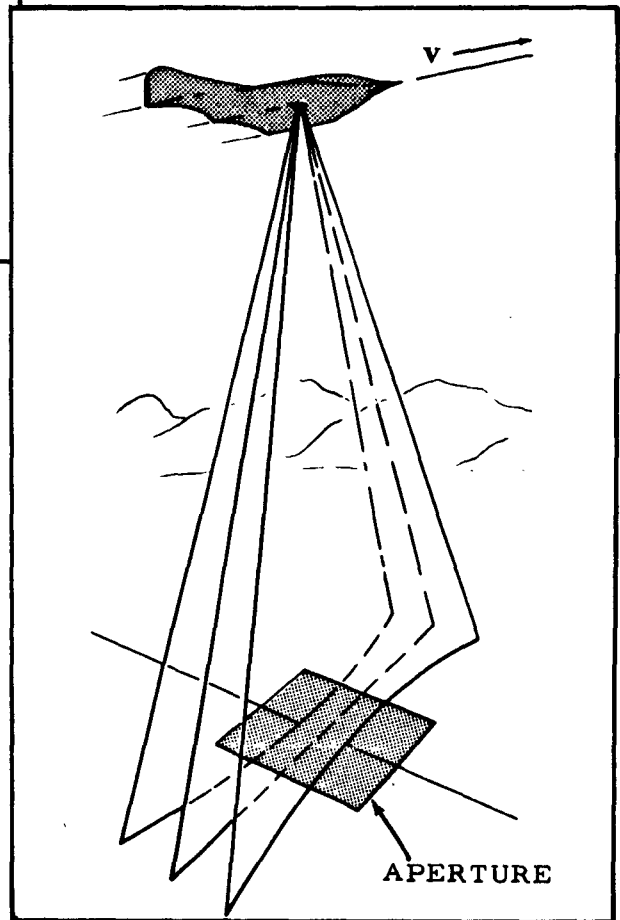
APERTURE

Figure 2b. Doppler Sampling Region on
a Planar Aperture

Using this physical picture, a simplification of Equation (12) can be made by recognizing that the limits of integration in t" are related to the filter time constant and that the time constant is proportional to the sampling region width divided by the probe velocity. For practical values of the sampling region width (1/10 to 1/100 of the aperture dimensions), the integrand can be approximated in a manner which is similar to the customary far field approximation of $\frac{\exp(-jkr)}{r}$. In the phase factor, let

$$\left\{ \left[v(t'' + t) - \eta \right]^2 + h^2 + \xi^2 \right\}^{1/2} \cong \left(h^2 + \xi^2 \right)^{1/2} \left[1 + \frac{vt''(vt - \eta)}{(h^2 + \xi^2)} \right] \tag{1}$$

and, in the amplitude factor, let

$$\frac{1}{\left\{ \left[v(t'' + t) - \eta \right]^2 + h^2 + \xi^2 \right\}^{1/2}} \cong \frac{1}{\left(h^2 + \xi^2 \right)^{1/2}} \tag{1}$$

With these substitutions, the integration in t" can be performed to give

$$S_{y_2}(t) = \frac{jk}{2\pi} \exp(j\omega_o t) \int_{\eta_1}^{\eta_2} d\eta \int_{c_1(\eta)}^{c_2(\eta)} d\xi F(\xi, \eta)$$

$$\cdot \exp\left[-jk\left(h^2 + \xi^2 \right)^{1/2} \right] \frac{\sin\left[\frac{kv}{2B} \frac{(vt - \eta)}{\left(h^2 + \xi^2 \right)^{1/2}} \right]}{kv(vt - \eta)} \tag{1}$$

11

The result is consistent with the physical operation of the system. The $\frac{\sin u}{u}$ function in the integrand is sharply peaked at $vt = \eta$ and has the effect of moving a sampling function across the aperture with a velocity v. The resolution of the sampling function is dependent on the parameters k, v, B, and h. The transverse aperture variable ξ also appears both in the sampling function and in the phase factor. In the sampling function, the effect is an aperture resolution which is a function of the transverse variable. This results from the fact that the lines on the aperture plane corresponding to constant Doppler frequency are hyperbolas rather than straight lines. The appearance of the variable ξ in the phase factor is caused by the fact that the probe antenna is in the near field of the transverse dimension of the sampling strip. This dependence is not required in the η dimension since the probe is in the far field for the width of the sampling strip in η.

To summarize, within the accuracy implicit in the approximations of Equations (13) and (14), Equation (15) represents the output signal from a rapidly moving Doppler antenna system as it passes over a general two-dimensional planar aperture. It has been assumed that the Doppler filter has $\frac{\sin u}{u}$ bandpass characteristics, and that the probe antenna has an omnidirectional lower hemisphere coverage and is moving with a constant velocity v at a constant height h.

III.   SPECIFIC APPLICATIONS

A large number of practical antennas may be represented mathe-matically by three planar configurations: (1) the line source, (2) the rectangular aperture with its aperture distribution separable in the orthogonal planes containing the major dimensions of the aperture, and (3) the circular aperture with a circularly symmetric aperture distribution.   The Transverse Doppler Pattern Measuring Technique has been applied to these configurations, and the results of the analytic investigations are presented below.

A.   Line Source with Uniform Phase

Perhaps the simplest aperture to consider is the line source with uniform phase.   In addition, a detailed study of the application of the measurement technique to the line source provides valuable information about basic system parameters.

For a line source of length a in η , Equation (15) reduces to

$$S_y(t) = \exp(j\omega_o t) \int_{-a/2}^{a/2} d\eta\, A(\eta)\, \frac{\sin\left[\dfrac{kv}{2Bh}(vt - \eta)\right]}{kv(vt - \eta)} \tag{1}$$

where a constant phase factor and a multiplicative constant have been omitted.   The aperture sampling function is

$$\frac{\sin\left[\dfrac{kv}{2Bh}(vt - \eta)\right]}{kv(vt - \eta)} \quad . \tag{1}$$

13

Determination of the optimum values of the parameter $\frac{kv}{2Bh}$ requires that Equation (16) be evaluated for the particular aperture distribution which is being measured. However, intuitive considerations can be used to approximate the parameters. If the aperture dimension is a, the resolution on the aperture can be expressed as a/N, where N is the number of sampling widths within the aperture. If the sampling resolution is chosen to be the 3 db width of the sampling function, the following relation of system parameters is obtained.

$$\frac{kva}{5.6\ BhN} = 1 \quad . \tag{18}$$

An additional constraint on the system parameters is imposed by the approximations made in the evaluation of the t'' integral in Equation (12). The "far zone" approximation of the integrand requires that

$$h > \frac{2\left(\frac{v}{B}\right)^2}{\lambda} \tag{19}$$

or

$$h = \frac{2a}{\lambda}\left(\frac{v}{B}\right)^2 \quad ; \quad a > 1 \quad . \tag{20}$$

When this condition is substituted in Equation (18), the equation takes the form

$$\frac{v}{B} = \frac{a}{N}\left(\frac{\pi}{5.6\ a}\right) \tag{21}$$

14

Therefore, the two equations governing the choice of the system parameters are

$$kh = \frac{a}{\pi}\left(\frac{kv}{B}\right)^2 \qquad (2?)$$

$$\frac{kv}{B} = \frac{ka}{N}\left(\frac{\pi}{5.6\,a}\right) \qquad (2?)$$

where the form of Equations (20) and (21) have been modified for convenience in graphing. These equations are plotted in Figures 3 and 4 with a as a parameter. The use of these curves to determine the operational parameters of the measuring system can be illustrated by a typical sample problem. Consider a line source 1000 feet in length operating at a wavelength of 2 feet:

ka = 3142 and, for a linear resolution corresponding to N = 10, ka/N = 314.2. From Figure 3 with a = 2, kv/B = 88.3. Thus, v/B = 28.1. If v = 600 mph = 880 ft/sec, B = 31 cps. From Figure 4, for kv/B = 88.3 and a = 2, kh = 4960, and h = 1580 feet.

Summarizing,

h = 1580 feet

v = 880 ft/sec

B = 31 cps

N = 10   .

It should be noted that the same value of a must be used for both graphs.
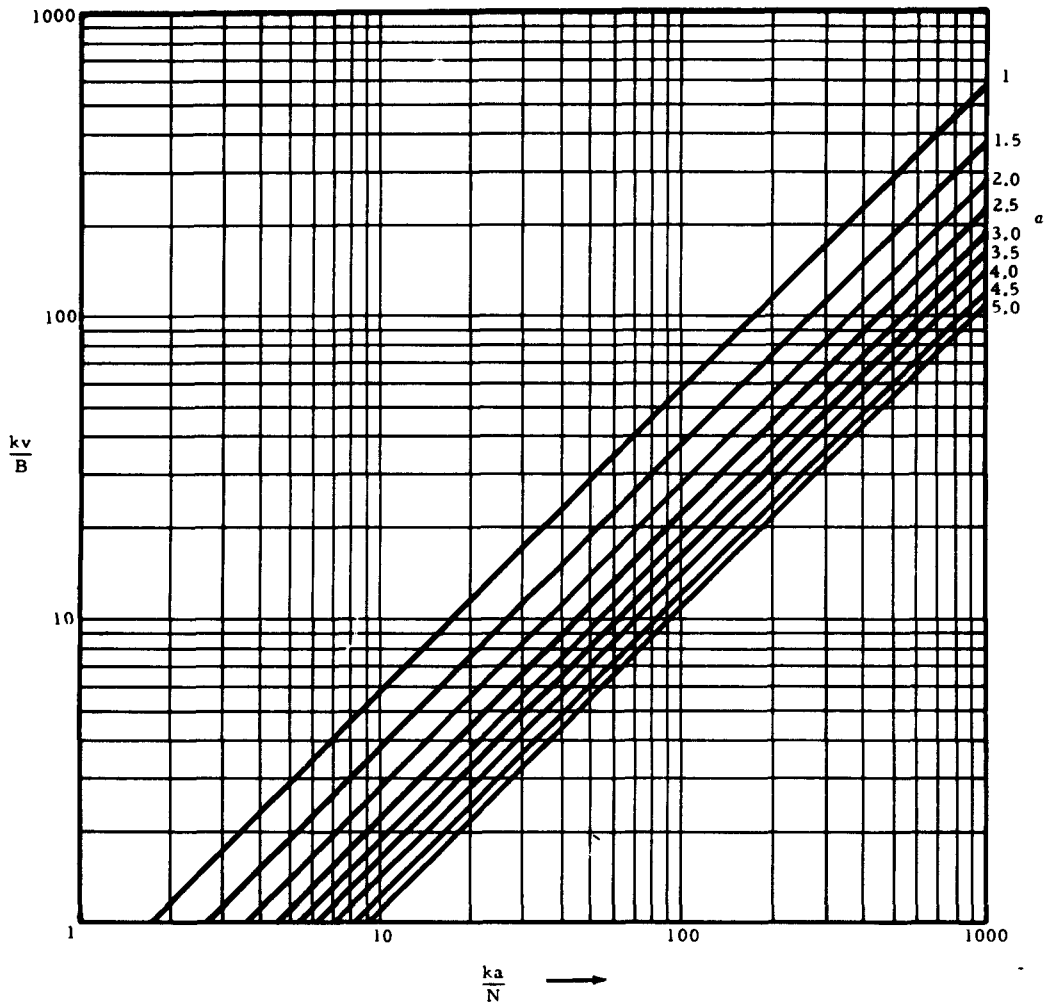
Figure 3. Relation Between $\frac{kv}{B}$ and $\frac{ka}{N}$ for $a \geq 1$
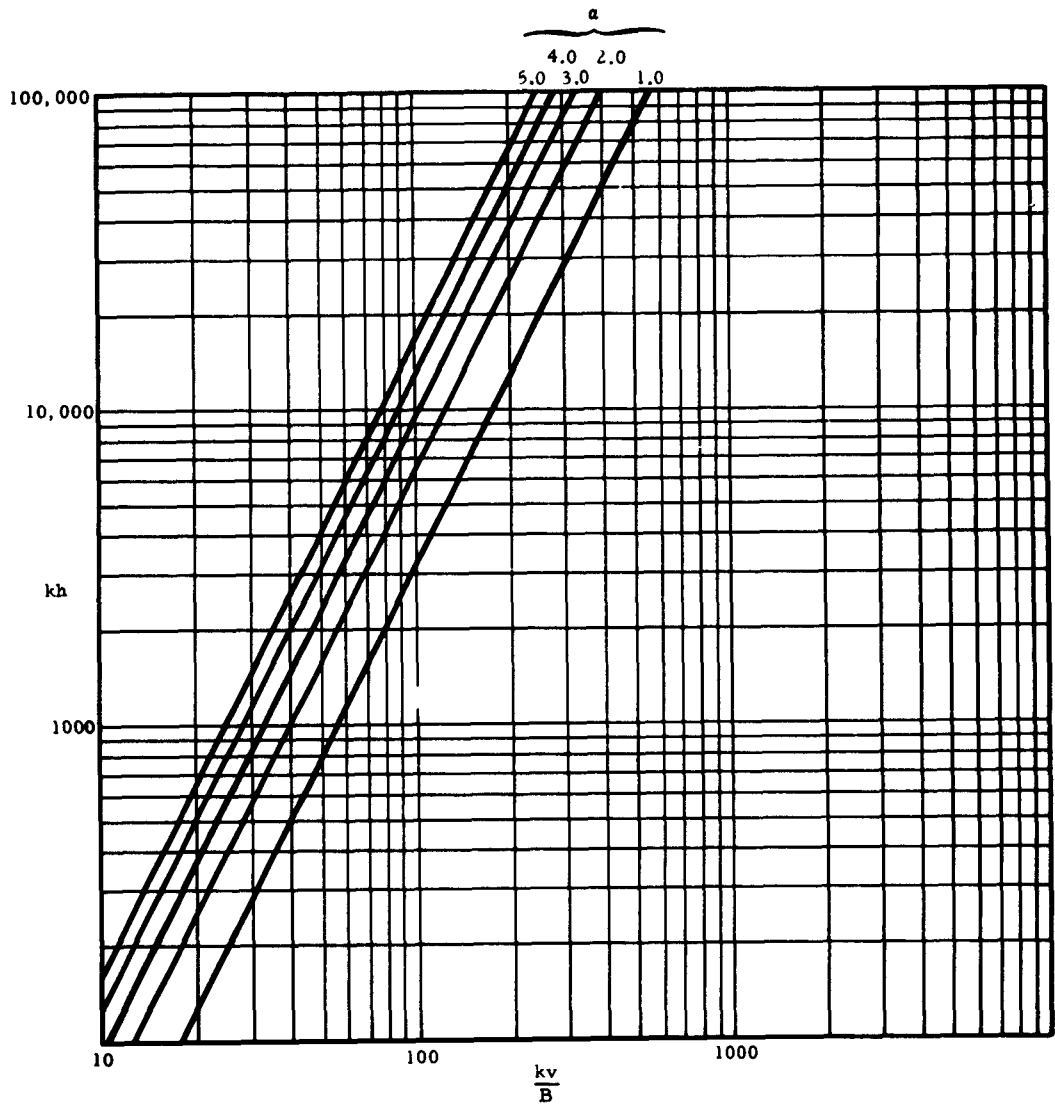
Figure 4.   Relation Between kh and $\dfrac{kv}{B}$ for $a \geq 1$

The above example indicates that the system designer has a considerable amount of latitude in choosing the system parameters provided the parameters are selected consistent with Equations (22) and (23).

To determine what effect the choice of the composite parameter $K = \frac{kva}{2Bh}$ has upon the accuracy with which the aperture distribution is reproduced, Equation (16) has been evaluated numerically in the form

$$S(\tau) = \int_{-1/2}^{1/2} A(\gamma) \frac{\sin\left[K(\tau - \gamma)\right]}{K(\tau - \gamma)} \, d\gamma \qquad (24$$

for various typical uniform phase line source distributions and values of the parameter K. The results of these calculations are presented in Scientific Report No. 1 on this contract on pages 19 through 23.[5] It can be seen that the accuracy with which the aperture distribution is measured increases as the value of K increases. This is as expected since increasing the value of K has the effect of narrowing the sampling function and correspondingly, the sampling width. In fact, it may be easily shown that, if the sampling function is the Dirac delta function (the case for $K \longrightarrow \infty$), the aperture distribution is measured exactly. It is also apparent that the best reproduction is obtained for those distributions which are zero at the ends of the aperture rather than for those which have abrupt discontinuities at the ends. This is to be expected from the analogy with Fourier representations of abruptly discontinuous functions.

B.   Rectangular Apertures with Separable Distributions and Uniform Phase

If the conditions for a rectangular aperture with a uniformly phased separable distribution, i.e.,

$$F(\xi, \eta) = f(\xi) f(\eta)$$

$$c_1(\eta) = -b/2$$

$$c_2(\eta) = b/2$$

$$\eta_1 = -a/2$$

$$\eta_2 = a/2$$

are introduced in Equation (15), it becomes

$$S_y(t) = \frac{jk}{2\pi} \exp(j\omega_o t) \int_{-a/2}^{a/2} d\eta\, f(\eta) \int_{-b/2}^{b/2} d\xi\, f(\xi) \, \exp\left[-jk\left(h^2 + \xi^2\right)^{1/2}\right]$$

$$\bullet \; \frac{\sin\left[\dfrac{kv}{2B} \dfrac{(vt - \eta)}{\left(h^2 + \xi^2\right)^{1/2}}\right]}{kv(vt - \eta)} \; .$$

(2

It should be noted, as mentioned above, that the transverse variable ξ appears in both the phase factor and the sampling function. However, for typical values of h and ξ, the variation in the sampling function resolution is less than one percent over the full excursion in ξ and may

19

be neglected with very little error. With this approximation Equation (25) may be written

$$S_y(t) = \frac{jk}{2\pi} \exp(j\omega_o t) \left\{ \int_{-b/2}^{b/2} d\xi f(\xi) \exp\left[-jk\left(h^2 + \xi^2\right)^{1/2}\right] \right\}$$

$$\bullet \int_{-a/2}^{a/2} d\eta f(\eta) \frac{\sin\left[\frac{kv}{2Bh}(vt - \eta)\right]}{kv(vt - \eta)} \,. \tag{26}$$

Thus the dependence in ξ appears only as a constant which modifies the amplitude of the expression. Therefore the discussion in the preceding section with regard to linear arrays may be applied directly to the consideration of rectangular apertures with separable distributions. A second measurement orthogonally oriented in space (with the roles of ξ and η in Equation (25) interchanged) is required to obtain the distribution in ξ.

C.   Nonuniformly Phased Linear and Separable, Rectangular Distributions

If, in Equation (16), the aperture excitation function is assumed to be complex, the equation has the form

$$S_y(t) = \exp(j\omega_o t) \int_{-a/2}^{a/2} d\eta A(\eta) \exp\left[j\phi(\eta)\right] \frac{\sin\left[\frac{kv}{2Bh}(vt - \eta)\right]}{kv(vt - \eta)} \tag{27}$$

where $F(\eta) = A(\eta) \exp\left[j\phi(\eta)\right]$. ($A(\eta)$ and $\phi(\eta)$ are real.) In particular for the usual linear phase shift required for scanning,

$$\phi(\eta) = \beta\eta \tag{2}$$

with β a constant. This equation has been evaluated numerically in the form

$$S(\tau) = \int_{-1/2}^{1/2} A(\gamma) \, \exp(j\beta\gamma) \, \frac{\sin\left[K(\tau - \gamma)\right]}{K(\tau - \gamma)} \, d\gamma \tag{2}$$

for two aperture distributions, uniform and $(1 - 2\gamma^2)$, and values of β corresponding to a total phase variation across the aperture of 1, 5, 10, and 20 radians. The results of the computations are presented on pages 28 through 36 of Scientific Report No. 1 on this contract.[5] In general, the reproductions of the amplitude compare favorably with those obtained for the in-phase apertures, and reproduction of the phase is excellent over the aperture. The exceptions occur for small values of K and $\beta = 20$. The relation of these parameters to the physic system may be determined from a consideration of Equation (18). Since $K = \frac{kva}{2\,Bh}$, we have

$$\frac{kva}{5.6\,BhN} = 1 = \frac{K}{2.8\,N} \tag{3}$$

or

$$N = \frac{K}{2.8} \tag{3}$$

where N is the number of sampling widths within the aperture. Therefore, a value of $K = 10$ corresponds to a sampling strip approximately 0.28 of the aperture dimension in width. Since the aperture phase slope

is 20 radians, there is a linear phase shift of 5.6 radians or almost a full cycle across each sampling width. It is not surprising, therefore, that the phase and amplitude resolution is poor for these values of the parameters.

The above values of phase variation over a large aperture correspond to relatively small scanning of the antenna beam. For example, for a 500λ aperture, $\beta = 20$ results in a scan of approximately two beamwidths. For scanning to an angle of 20° (of the order of 120 beamwidths), a value of $\beta \cong 1075$ is required. Numerical evaluations of Equation (31) for this value of β and several distribution parameters were also performed. These are definitely unsatisfactory with regard to both phase and amplitude. As discussed above, however, this is not unexpected. Even for $K = 60$, corresponding to approximately 21.4 sampling widths within the aperture, there is a phase slope of approximately 50 radians across a sampling strip. Since the signal out of the filter is essentially an average signal from the sampling strip, it can be shown that the amplitude of the signal tends to be zero except near the edges of the aperture where a nonsymmetrical condition exists with respect to the sampling function.

D. Circular Aperture with a Circularly Symmetric Aperture Distribution

For a circular aperture of radius $a/2$ with a circularly symmetric aperture distribution, Equation (15) has the form

$$S_y(t) = \frac{jk}{2\pi} \exp(j\omega_o t) \int_{-a/2}^{a/2} d\eta \int_{-\sqrt{(a/2)^2 - \eta^2}}^{\sqrt{(a/2)^2 - \eta^2}} d\xi F(\xi, \eta)$$

$$\bullet \exp\left[-jk\left(h^2 + \xi^2\right)^{1/2}\right] \frac{\sin\left[\frac{kv}{2B} \frac{(vt - \eta)}{\left(h^2 + \xi^2\right)^{1/2}}\right]}{kv(vt - \eta)} \tag{32}$$

where $F(\xi, \eta)$ is circularly symmetric in ξ and η. This expression poses considerable difficulty from a computational standpoint. The problems arise basically from the facts that Equation (32) contains a double integral and approximately N^2 summations are required in its numerical evaluation (as compared to N summations for a one-dimensional integral) and, secondly, that the phase factor containing $\left(h^2 + \xi^2\right)^{1/2}$ varies over a wide range during the transverse integration necessitating the use of a large number of increments in performing the summation. Some effort has been expended on obtaining an alternate formulation of Equation (32) which is more amenable to computer programming. The results of this work appears in Appendix A.

However, a more fruitful approach has been developed utilizing both mathematical and physical modifications. This development is presented in Section IV. A.

IV.   ALTERNATE SIGNAL PROCESSING TECHNIQUE

A.   Multichannel Signal Processing

As was stated in the previous section, the difficulty in evaluating the general sampling function equation is due primarily to the presence of both space and time variables in the integrands of the Fourier transform pairs. In the analysis that follows, alternate approximations are applied which allow the time variable to be transformed into the aperture distribution, and the transverse variable ξ is eliminated using the directional characteristics of a linear array sampling antenna. The effect of varying the filter center frequency is also examined by means of a more generalized filter function.   The significance of these modifications is discussed below.

Starting with Equation (8), let

$$H(\omega) \; = \; \frac{\sin\left(\dfrac{\omega - \omega_n}{2B}\right)}{\omega - \omega_n}$$

where

B = bandwidth

ω_n = center frequency, n = 1, 2, 3, . . . , N.

For this condition, Equation (8) becomes

$$S_y(t) = \frac{j}{(2\pi)^2} \int_{\eta_1}^{\eta_2} d\eta \int_{c_1(\eta)}^{c_2(\eta)} d\xi F(\xi, \eta) \int_{-\infty}^{\infty} \frac{\sin\left(\frac{\omega - \omega_n}{2B}\right)}{\omega - \omega_n} \exp\left[j\omega(t - t')\right] d\omega$$

$$\cdot \int_{-\infty}^{\infty} k \frac{\exp\left[-jk\sqrt{(vt' - \eta)^2 + h^2 + \xi^2}\right]}{\sqrt{(vt' - \eta)^2 + h^2 + \xi^2}} \exp(j\omega_o t')\, dt' \qquad . \qquad (33)$$

Since

$$\int_{-\infty}^{\infty} \frac{\sin\left(\frac{\omega - \omega_n}{2B}\right)}{\omega - \omega_n} \exp\left[j\omega(t - t')\right] d\omega = \pi \exp\left[-j\omega_n(t' - t)\right] \qquad t - \frac{1}{2B} \le t' \le t + \frac{1}{2B}$$

$$= 0 \qquad \qquad \text{for all other } t',$$

Equation (33) becomes

$$S_y(t) = \frac{j}{4\pi} \int_{\eta_1}^{\eta_2} d\eta \int_{c_1(\eta)}^{c_2(\eta)} d\xi F(\xi, \eta) \int_{t - 1/2B}^{t + 1/2B} k$$

$$\cdot \frac{\exp\left[-jk\sqrt{(vt' - \eta)^2 + h^2 + \xi^2}\right]}{\sqrt{(vt' - \eta)^2 + h^2 + \xi^2}} \exp\left[j(\omega_o - \omega_n)\right]t' \ \exp(-j\omega_n t)\, dt' \qquad . \qquad (34)$$

With the change of variable

$$t' = t'' + t$$

$$dt' = dt'' \quad ,$$

Equation (34) becomes

$$S_y(t) = \frac{j}{4\pi} \int_{\eta_1}^{\eta_2} d\eta \int_{c_1(\eta)}^{c_2(\eta)} d\xi F(\xi, \eta) \int_{-1/2B}^{1/2B} k$$

$$\cdot \frac{\exp\left\{-jk\sqrt{[v(t''+t) - \eta]^2 + h^2 + \xi^2}\right\}}{\sqrt{[v(t''+t) - \eta]^2 + h^2 + \xi^2}} \exp\left[j\omega_o(t''+t)\right] \exp(-j\omega_n t'') \, dt'' \quad . \quad (35$$

The radical

$$\sqrt{[v(t''+t) - \eta]^2 + h^2 + \xi^2} = \sqrt{h^2 + \xi^2 + (\eta - vt)^2 + (vt'')^2 - 2vt''(\eta - vt)} \quad\quad (36$$

can be approximated by

$$\sqrt{h^2 + \xi^2 + (vt - \eta)^2} - \frac{vt''(\eta - vt)}{\sqrt{h^2 + \xi^2 + (\eta - vt)^2}} \quad\quad (37$$

in the exponent and

$$\sqrt{h^2 + \xi^2 + (\eta - vt)^2} \tag{38}$$

in the denominator. These approximations of course impose certain limitations on the functions vt" and (vt - η). In particular, the expression $(vt")^2$ has been ignored completely in both the phase and amplitude factor. It is seen from Equation (36) that this term has its greatest effect at (vt - η) = 0 and $\xi = 0$. This is comparable to the on-axis quadratic phase error of a linear array, where in this case, the "linear array" is the flight path $\frac{v}{B}$ as illustrated in Figure 5. The maximum dimension of the "array" is $\frac{v}{B}$, and if the quadratic phase error is to be ignored, this dimension must be limited.[4]
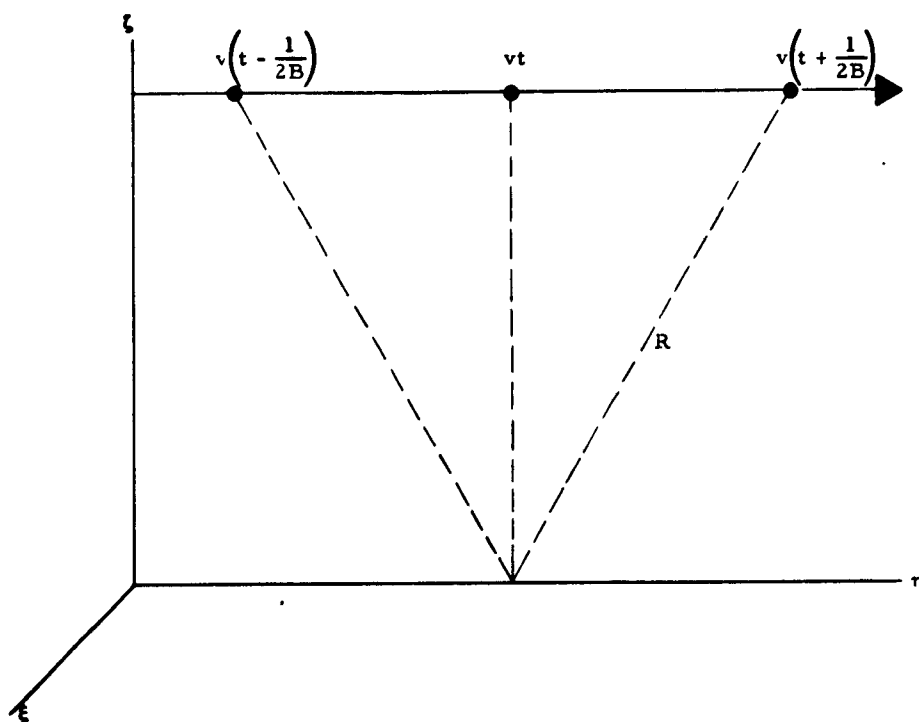
Figure 5. Variations in R Associated with the Flight Path Length $\frac{v}{B}$

Referring to Figure 6,

$$h^2 + \left(\frac{v}{2B}\right)^2 = R^2 = (h + \Delta R)^2$$

$$h^2 + \left(\frac{v}{2B}\right)^2 = h^2 + (\Delta R)^2 + 2h\Delta R \quad .$$

Where ΔR is small enough to allow the deletion of $(\Delta R)^2$, then

$$\left(\frac{v}{2B}\right)^2 = 2h\Delta R \quad .$$

Using a $\frac{\lambda}{8}$ criteria for the maximum allowable phase error produces

$$\left(\frac{v}{2B}\right)^2 = (vt'')^2_{max} = 2h\,\frac{\lambda}{8} = \frac{\lambda h}{4} \quad .$$
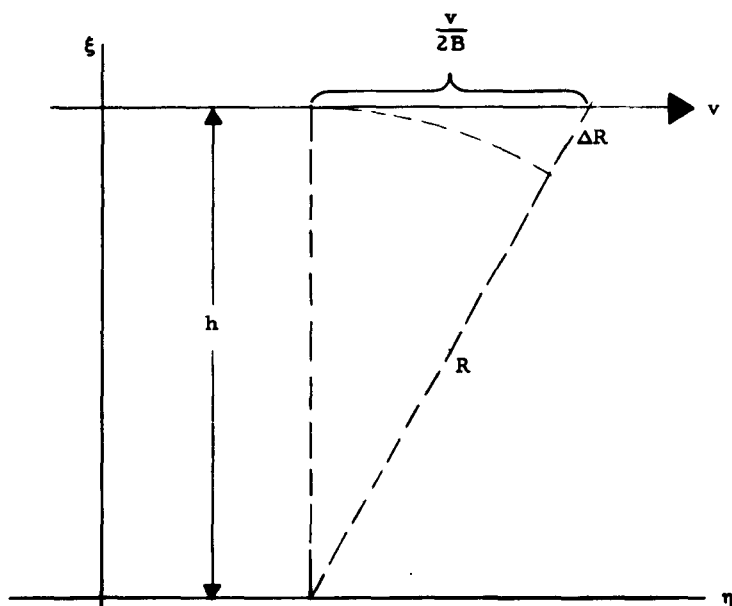
Figure 6. Geometry for Determining the Limits on B

This forces the condition

$$B \geq \frac{v}{\sqrt{h\lambda}}$$

on B. For $v = 880$ feet per second, $h = 1580$ feet, and $\lambda = 2$ feet

$$B \geq \frac{880}{\sqrt{3160}} = 15.6 \text{ cycles}$$

which is compatible with the conditions of Section III. A. Since it has been shown that the range of $(\eta - vt)$ is limited in the ξ, η plane, Equations (37) and (38) are comparable to the usual far field approximations. Under these conditions, Equation (35) can be integrated with respect to t'' to give

$$S_y(t) = \frac{j \exp(j\omega_o t)}{4\pi B} \int_{\eta_1}^{\eta_2} d\eta \int_{c_1(\eta)}^{c_2(\eta)} d\xi F(\xi, \eta) k$$

$$\cdot \frac{\exp\left[-jk\sqrt{h^2 + \xi^2 + (\eta - vt)^2}\right]}{\sqrt{h^2 + \xi^2 + (\eta - vt)^2}} \frac{\sin\left\{\frac{1}{2B}\left[\frac{kv(\eta - vt)}{\sqrt{h^2 + \xi^2 + (\eta - vt)^2}} + \omega_o - \omega_n\right]\right\}}{\frac{1}{2B}\left[\frac{kv(\eta - vt)}{\sqrt{h^2 + \xi^2 + (\eta - vt)^2}} + \omega_o - \omega_n\right]} \quad (39)$$

Equation (39) differs from Equation (15) in that the term $(\eta - vt)^2$ appears under the radical and the term $\omega_o - \omega_n$ is present in the $\frac{\sin u}{u}$ sampling function. The significance of the former will become more apparent as

29

the analysis continues. Regarding the term $\omega_o - \omega_n$, it is apparent that this factor shifts the peak of the $\frac{\sin u}{u}$ functions in the η direction ahead or behind the zero Doppler frequency trace as ω_n is greater than or less than ω_o. Figure 7 illustrates the result of passing the received signal through a multichannel filter bank. By proper choice of filter frequencies, the ξ, η plane has been divided into strips where the output of the nth filter is the signal transmitted from the nth Doppler frequency trace. The presence of the term $(\eta - vt)$ verifies mathematically that the sampling system is of a traveling nature; i.e., with the exception of the aperture distribution function, $F(\xi, \eta)$, each factor in the integrand of Equation (39) is a traveling function with velocity v in the η direction.
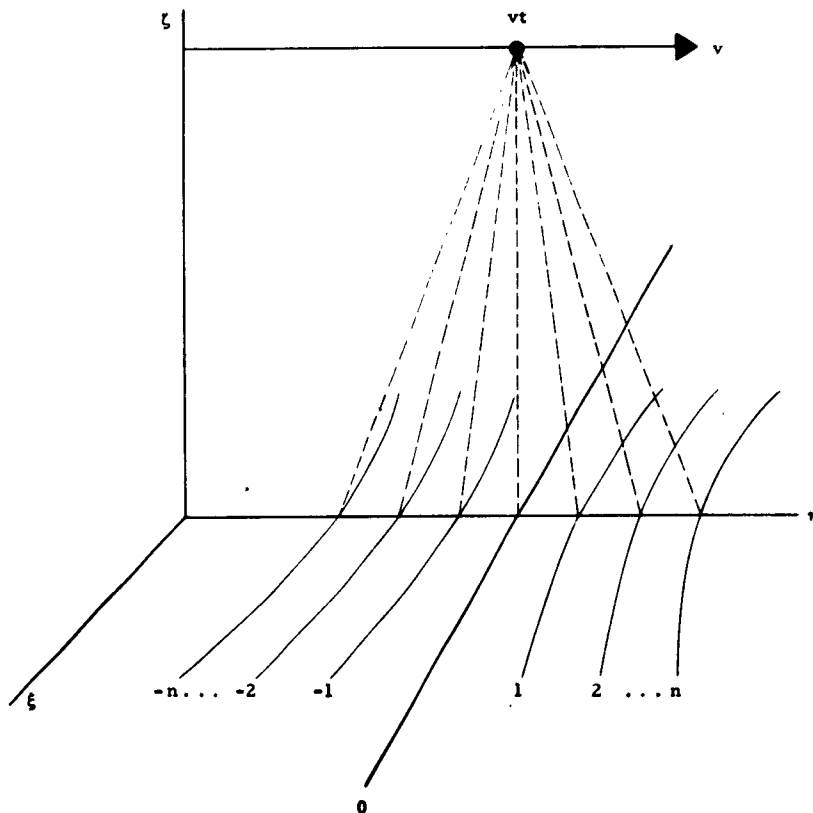
Figure 7. Sampling Strips Produced by a Multichannel Filter Bank

At this point it is advantageous to introduce the effect of replacing the omnidirectional sampling probe with a linear array. Figure 8 illustrates the geometry of a linear array and its trace in the (ξ, η) plane. The array is oriented at the point $(0, 0, h)$ in the ξ, η, ζ coordinate system with its longitudinal axis parallel to the ξ axis. For an assumed $\frac{\sin u}{u}$ pattern, the argument u takes the form

$$u = \frac{\pi L}{\lambda_o} \sin \beta \quad ,$$

where L is the length of the array and β is the broadside angle measured from the ζ, η plane.
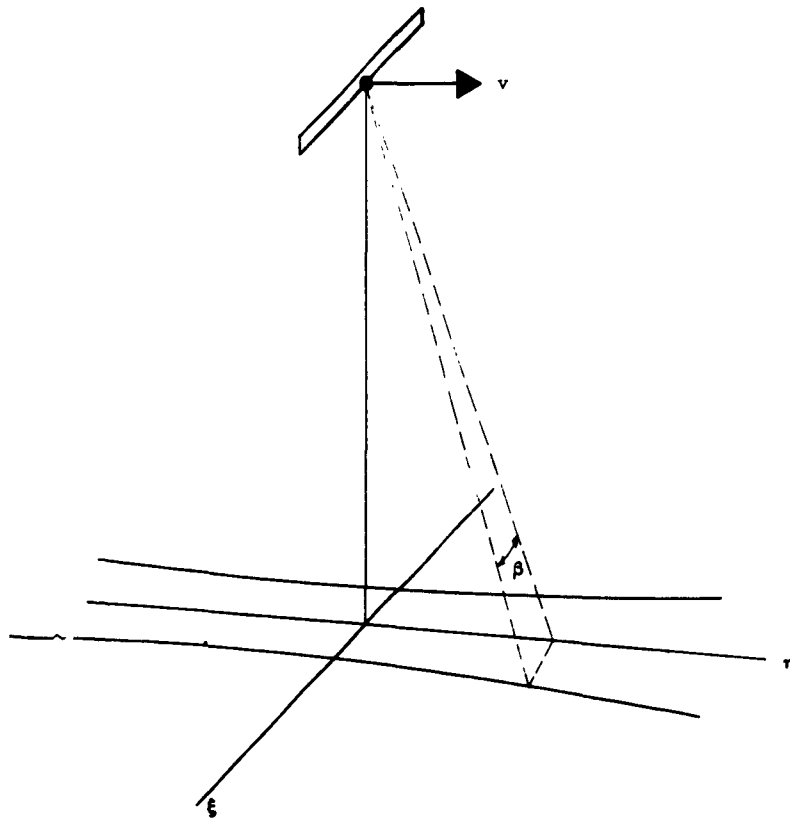
Figure 8. ξ, η Trace of a Linear Array Sampling Antenna

Under these conditions the weighting effect of the array on a signal received from the ξ, η plane can be expressed as,

$$W_2' = \frac{\sin\left\{\dfrac{\pi L}{\lambda}\ \dfrac{\xi}{\sqrt{h^2 + \xi^2 + \eta^2}}\right\}}{\dfrac{\pi L}{\lambda}\ \dfrac{\xi}{\sqrt{h^2 + \xi^2 + \eta^2}}}\ \frac{1}{\sqrt{h^2 + \xi^2 + \eta^2}}$$ (40)

where the space attenuation factor

$$\frac{1}{\sqrt{h^2 + \xi^2 + \eta^2}}$$

has been included. Equation (40) can now be generalized by rotating the trace about the ζ axis through an angle a and then translating the skewed strip along the η axis by the time function vt. The resulting expression

$$W_2 = \frac{\sin\left\{\dfrac{\pi L}{\lambda}\left[\dfrac{\xi \cos a - (\eta - vt) \sin a}{\sqrt{h^2 + \xi^2 + (\eta - vt)^2}}\right]\right\}}{\dfrac{\pi L}{\lambda}\left[\dfrac{\xi \cos a - (\eta - vt) \sin a}{\sqrt{h^2 + \xi^2 + (\eta - vt)^2}}\right]}$$

represents the trace of a linear array carried by the mapping vehicle at an angle a with respect to the direction of motion. Under these conditions the expression for the filtered signal is

32

$$g(t) = \frac{j \exp(j\omega_o t)}{4\pi B} \int_{\eta_1}^{\eta_2} \int_{c_1(\eta)}^{c_2(\eta)} F(\xi, \eta) \; \frac{\exp(-jkr')}{(r')^2}$$

$$\cdot \; \frac{\sin\left\{\dfrac{1}{2B}\left[\dfrac{kv(\eta - vt)}{\sqrt{h^2 + \xi^2 + (\eta - vt)^2}} + \omega_o - \omega_n\right]\right\}}{\dfrac{1}{2B}\left[\dfrac{kv(\eta - vt)}{\sqrt{h^2 + \xi^2 + (\eta - vt)^2}} + \omega_o - \omega_n\right]} \; \frac{\sin\left\{\dfrac{\pi L}{\lambda}\left[\dfrac{\xi \cos a - (\eta - vt)\sin a}{\sqrt{h^2 + \xi^2 + (\eta - vt)^2}}\right]\right\}}{\dfrac{\pi L}{\lambda}\left[\dfrac{\xi \cos a - (\eta - vt)\sin a}{\sqrt{h^2 + \xi^2 + (\eta - vt)^2}}\right]} \; d\xi d\eta$$

(41

where

$$(r')^2 = h^2 + \xi^2 + (\eta - vt)^2 \qquad .$$

Figure 9 illustrates the limiting effect of both the filter function and the pattern factor of the sampling array. It is seen that the array has re-duced the sampling strip produced by the filter to a sampling increment with dimensions in the ξ direction comparable to those in the η direc-tion. Hence far field approximations can now be made in the function

$$\frac{\exp(-jkr')}{(r')^2}$$

with respect to both ξ and η.

In order to select a suitable coordinate system for the far field expression, attention is directed to the point $(\xi_o, \eta_o' + vt)$ in Figure 9. This point is the intersection of the two lines along which the two $\dfrac{\sin u}{u}$ terms in Equation (41) have maximum values. Hence, for
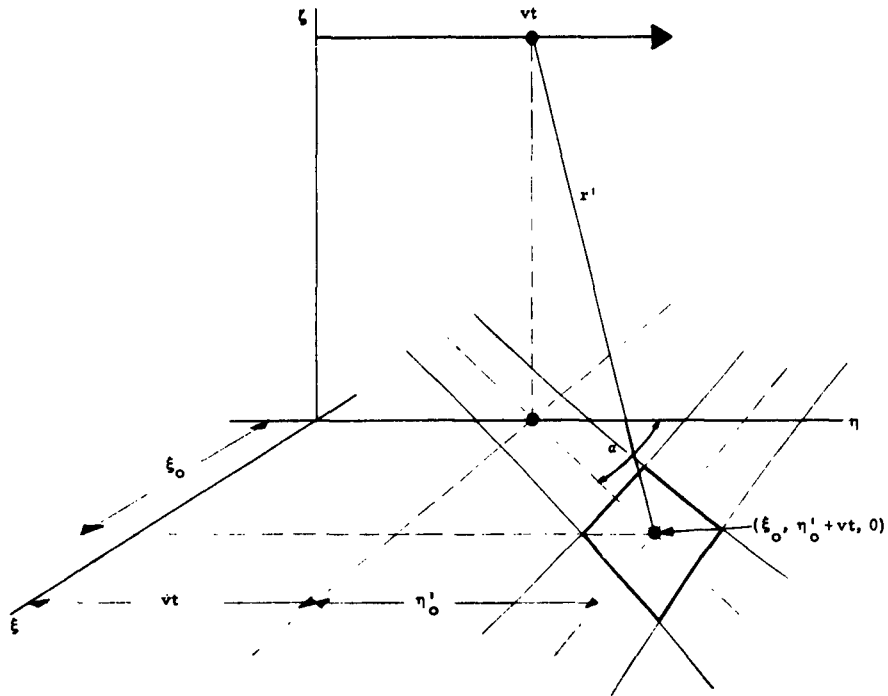
Figure 9.   Incremental Sampling Area Isolated by the Filter
Function and Sampling Array Pattern Factor

given values of L, ω_o, ω_n, and a, the coordinates ξ_o and η_o' can be computed by equating each $\dfrac{\sin u}{u}$ argument to zero and then solving the two simultaneous equations for ξ and $\eta - vt$ as follows.   From

$$\frac{1}{2B}\left[\frac{kv(\eta - vt)}{\sqrt{h^2 + \xi^2 + (\eta - vt)^2}} + \omega_o - \omega_n\right] = 0$$

and

$$\frac{\pi L}{\lambda}\left[\frac{\xi \cos a - (\eta - vt) \sin a}{\sqrt{h^2 + \xi^2 + (\eta - vt)^2}}\right] = 0 \quad ,$$

34

$$(\eta - vt)^2 = \frac{h^2(\omega_n - \omega_o)^2}{(kv)^2 - (\omega_n - \omega_o)^2 \sec^2 a} = (\eta_o')^2 \qquad (42$$

$$\xi^2 = \frac{h^2(\omega_n - \omega_o)^2 \tan^2 a}{(kv)^2 - (\omega_n - \omega_o)^2 \sec^2 a} = \xi_o^2 \qquad (43$$

The far field approximations in polar coordinates can now be constructed for

$$\frac{\exp(-jkr')}{(r')^2}$$

at the (ξ, η, ζ) origin and then translated to the point $(\xi_o, \eta_o' + vt, 0)$ as follows:

At the point $(0, 0, 0)$[4]

$$\frac{\exp(-jkr')}{(r')^2} \approx \frac{\exp(-jkR)}{R^2} \exp\left\{jk \sin\theta \left[\xi \cos\phi + \eta \sin\phi\right]\right\}$$

where R is a constant slant range and θ and ϕ are the familiar azimuth and coelevation coordinates illustrated in Figure 10.
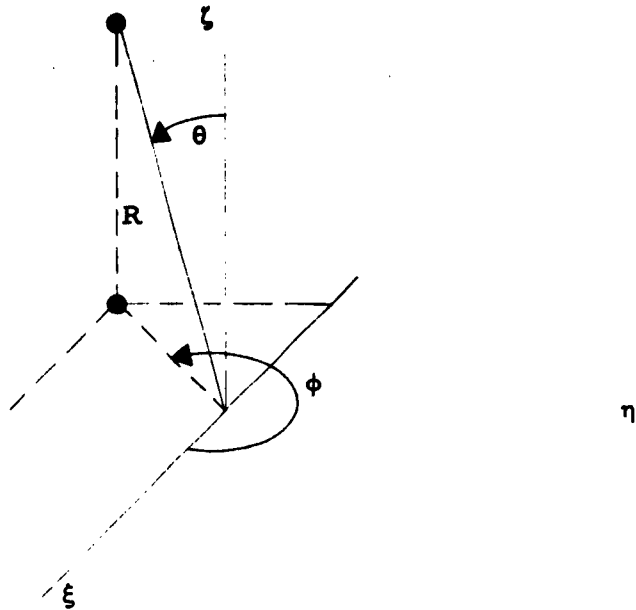
Figure 10.   Polar Coordinates for the Far Field Approximations
Referred to the ξ, η, ζ Origin

At the point $(\xi_o, \eta'_o + vt, 0)$

$$\frac{\exp(-jkr')}{(r')^2} \approx \frac{\exp(-jkR)}{R^2} \exp\left(jk\sin\theta\left\{(\xi - \xi_o)\cos\phi + \left[\eta - (\eta'_o + vt)\right]\sin\phi\right\}\right)$$

where now

$$R = \sqrt{h^2 + \xi_o^2 + (\eta'_o)^2} = \frac{hkv}{\sqrt{(kv)^2 - (\omega_n - \omega_o)^2 \sec^2 \alpha}} \qquad . \tag{44}$$

The result of this translation is illustrated in Figure 11.   Equation (41)
now becomes
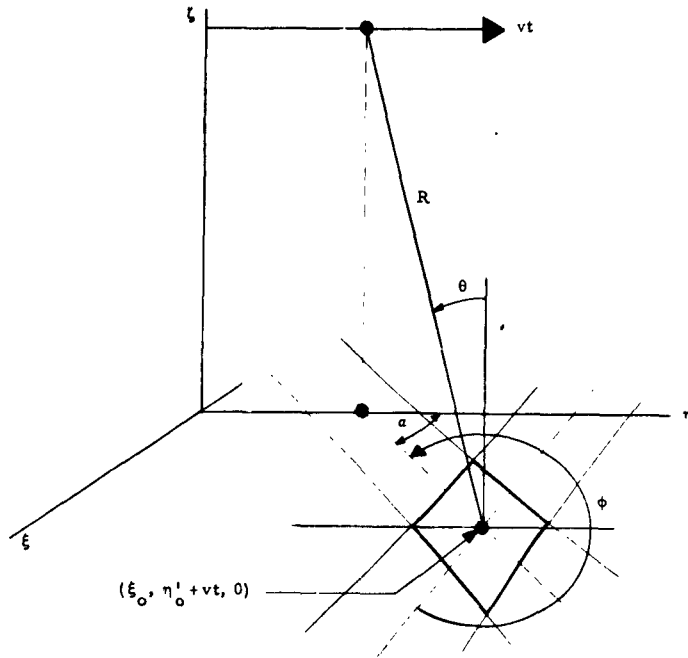
Figure 11.   Polar Coordinates for the Far Field Approximations
Referred to the Point $(\xi_o, \ \eta_o' + vt, \ 0)$

$$g(t) = \frac{j \exp (j\omega_o t)}{4\pi B} \ \frac{\exp (-jkR)}{R^2} \int_{\eta_1}^{\eta_2} \int_{c_1(\eta)}^{c_2(\eta)} F(\xi, \eta)$$

$$\bullet \exp\left(jk \sin \theta \left\{(\xi - \xi_o) \cos \phi + \left[\eta - (\eta_o' + vt)\right] \sin \phi\right\}\right) W_1 W_2 \ d\xi d\eta$$

where

$$W_1 = \frac{\sin\left\{\dfrac{1}{2B}\left[\dfrac{kv(\eta - vt)}{\sqrt{h^2 + \xi^2 + (\eta - vt)^2}} + \omega_o - \omega_n\right]\right\}}{\dfrac{1}{2B}\left[\dfrac{kv(\eta - vt)}{\sqrt{h^2 + \xi^2 + (\eta - vt)^2}} + \omega_o - \omega_n\right]}$$

37

$$W_2 = \frac{\sin\left\{\frac{\pi L}{\lambda}\left[\dfrac{\xi\cos\alpha - (\eta - vt)\sin\alpha}{\sqrt{h^2 + \xi^2 + (\eta - vt)^2}}\right]\right\}}{\dfrac{\pi L}{\lambda}\left[\dfrac{\xi\cos\alpha - (\eta - vt)\sin\alpha}{\sqrt{h^2 + \xi^2 + (\eta - vt)^2}}\right]} \tag{4}$$

Although mathematically unwieldy, Equation (45) yields considerable information as to the nature of the sampling system output. From previous experience with the analysis of illuminated apertures, Equation (45) is recognized as the far field diffraction integral of an irregular shaped aperture with a tapered distribution. The weighting functions, W_1 and W_2, clearly have a tapering effect on the distribution function $F(\xi, \eta)$, and for a chosen attenuation criteria establish the boundaries of the isolated area in the ξ, η plane. It is again emphasized that the presence of the term $(\eta - vt)$ establishes the traveling nature of the integrand; i.e., the isolated area centered at the point $(\xi_o, \eta_o' + vt, 0)$, the slant range R, and the vehicle position vt are all fixed with respect to each other and travel at a constant velocity v in the η direction.

Because of the time dependence of the sampling function, the limits of the integral and hence the distribution function, $F(\xi, \eta)$, are also functions of time. This can be illustrated by making the approximations in the arguments of the $\frac{\sin u}{u}$ functions,.

$$\sqrt{h^2 + \xi^2 + (\eta - vt)^2} \approx \sqrt{h^2 + \xi_o^2 + \eta_o'^2} = R \tag{4}$$

which is valid for small variations in ξ and η about ξ_o and η_o'. Now

$$W_1 \approx \frac{\sin\left\{\frac{1}{2B}\left[\frac{kv(\eta - vt)}{R} + \omega_o - \omega_n\right]\right\}}{\frac{1}{2B}\left[\frac{kv(\eta - vt)}{R} + \omega_o - \omega_n\right]} \qquad (49)$$

$$W_2 \approx \frac{\sin\left\{\frac{\pi L}{\lambda}\left[\frac{\xi \cos \alpha - (\eta - vt)\sin \alpha}{R}\right]\right\}}{\frac{\pi L}{\lambda}\left[\frac{\xi \cos \alpha - (\eta - vt)\sin \alpha}{R}\right]} \qquad (50)$$

Figure 12 illustrates the sampling increment under the conditions of Equation (48). The point, $(\xi_o, \eta_o' + vt)$, has been computed in Equations (42) and (43).
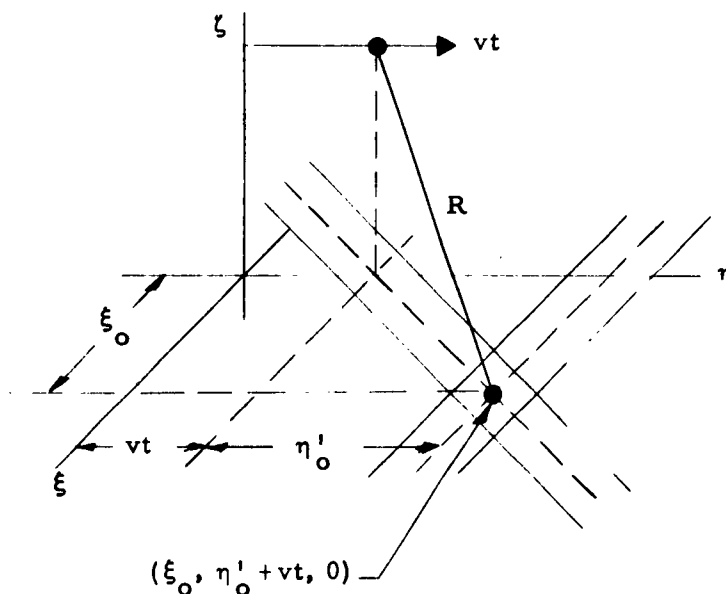
Figure 12. Incremental Sampling Area Using a Constant Value of R in the Filter and Array Functions

Using the 3 db attenuation criteria, the limits on ξ and η are computed from

$$\frac{1}{2B}\left[\frac{kv(\eta - vt)}{R} + \omega_o - \omega_n\right] = \pm 1.39 \tag{5}$$

and

$$\frac{\pi L}{\lambda}\left[\frac{\xi \cos a - (\eta - vt)\sin a}{R}\right] = \pm 1.39 \quad . \tag{5}$$

From which follows

$$\eta - vt = \pm \frac{R}{kv} 2.78B + \frac{R}{kv}(\omega_n - \omega_o)$$

$$= \pm \frac{R}{kv} 2.78B + \eta_o' \tag{5}$$

and

$$\xi = \pm 1.39 \frac{R\lambda}{\pi L}\sec a + (\eta - vt)\tan a \quad . \tag{54}$$

Under these conditions, the limits of integration in Equation (42) are

$$c_1(\eta) = (\eta - vt)\tan a - 1.39\frac{R\lambda}{\pi L}\sec a$$

$$c_2(\eta) = (\eta - vt)\tan a + 1.39\frac{R\lambda}{\pi L}\sec a$$

where

$$\eta_1 = vt + \eta_0' - \frac{R}{kv} 2.78 \, B$$

$$\eta_2 = vt + \eta_0' + \frac{R}{kv} 2.78 \, B \quad .$$

It is seen that the limits on ξ are a linear function of η and t, and η varies symmetrically about a particular value, $(vt + \eta_0')$, which is a function of the time variable. Hence the distribution function $F(\xi, \eta)$ is necessarily a function of t because of the nature of the limits of integration. This result can be obtained in a more straightforward manner by the change of variable

$$\eta = \eta' + vt \quad . \tag{5}$$

Substituting the conditions of Equations (48) and (55) into Equation (45) produces

$$g(t) = \frac{j \exp\left[j(\omega_0 t - kR)\right]}{4\pi B R^2} \int_{\eta_1'}^{\eta_2'} \int_{c_1'(\eta')}^{c_2'(\eta')} F(\xi, \eta' + vt)$$

$$\bullet \exp\left(jk \sin \theta \left\{(\xi - \xi_0) \cos \phi + (\eta' - \eta_0') \sin \phi\right\}\right) W_1 W_2 \, d\xi d\eta' \tag{5}$$

where

$$W_1 = \frac{\sin \frac{1}{2B}\left[\frac{kv\eta'}{R} + \omega_0 - \omega_n\right]}{\frac{1}{2B}\left[\frac{kv\eta'}{R} + \omega_0 - \omega_n\right]} \tag{5}$$

41

$$W_2 = \frac{\sin \frac{\pi L}{\lambda}\left[\frac{\xi \cos \alpha - \eta' \sin \alpha}{R}\right]}{\frac{\pi L}{\lambda}\left[\frac{\xi \cos \alpha - \eta' \sin \alpha}{R}\right]}$$

<div style="text-align:right">(5</div>

$$c_1'(\eta') = \eta' \tan \alpha - 1.39 \frac{R\lambda}{\pi L} \sec \alpha$$

$$c_2'(\eta') = \eta' \tan \alpha + 1.39 \frac{R\lambda}{\pi L} \sec \alpha$$

$$\eta_1' = \eta_o' - \frac{R}{kv} (2.78) B$$

$$\eta_2' = \eta_o' + \frac{R}{kv} (2.78) B \quad .$$

<div style="text-align:right">(5</div>

It is seen that the change of variable of Equation (55) has essentially transformed the time variable, t, into the aperture distribution function, while at the same time removing it from the remaining factors and limits of the diffraction integral. This is in complete agreement with the foregoing discussion; i.e., at any instant of time the output of the filter represents the weighted aperture distribution, $F(\xi, \eta' + vt)$, integrated over the limits,

$$\xi = \eta' \tan \alpha \pm 1.39 \frac{R\lambda}{\pi L} \sec \alpha$$

and

$$\eta = \eta' + vt = \eta_o' + vt \pm \frac{R}{kv} (2.78) B \quad .$$
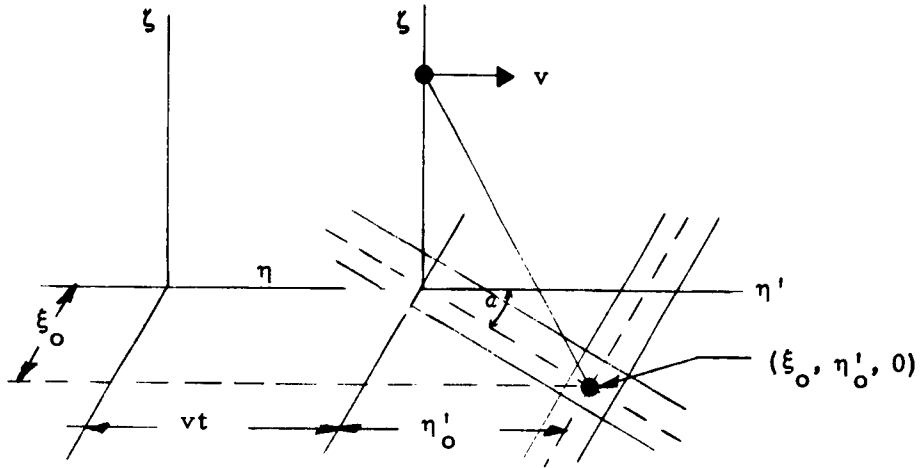
Figure 13.   Geometry of the Moving Reference Frame, (ξ, η', ζ), and the Fixed Frame (ξ, η, ζ)

Equations (56) through (59) can be interpreted as the far field expression for a radiating aperture referred to as a moving reference frame, i.e., the coordinate frame of the sampling system.   In the ξ, η' plane, the incremental area is a parallelogram centered at the point $\xi = \xi_0$ and $\eta' = \eta'_0$ as illustrated in Figure 13.   Equations (42) and (43) give the values of η'_0 and ξ_0 in terms of the parameters h, ω_0, ω_n, v, and a. Hence, it follows that for fixed values of h, ω_0, v, and a, variations in the parameter ω_n produce a shift in the position of the point (ξ_0, η'_0) along the line $\xi = \eta'$ tan a.   For the case of the multichannel filterbank discussed previously, the trace of the linear array is divided up into N sampling increments.   The output of the nth filter is in the form of Equation (53) where the aperture distribution is now clearly a function of time.   The output of the nth filter can now be expressed as

$$g_n(t) = \frac{j \exp\left[j(\omega_o t - kR_n)\right]}{4B\pi R_n^2} \int_{\eta'_n - \frac{R_n}{kv}(2.78B)}^{\eta'_n + \frac{R_n}{kv}(2.78B)} d\eta'$$

$$\bullet \int_{\eta' \tan a - 1.39 \frac{R_n \lambda}{\pi L} \sec a}^{\eta' \tan a + 1.39 \frac{R_n \lambda}{\pi L} \sec a} d\xi$$

$$\bullet \exp\left(jk \sin\theta \left\{(\xi - \xi_n)\cos\phi + (\eta' - \eta'_n)\sin\phi\right\}\right) F(\xi, \eta' + vt) W_1 W_2 \qquad (6$$

where W_1 and W_2 differ from Equations (57) and (58) only in that R is replaced by R_n to denote the nth filter output.

Figure 14 illustrates the geometry of a multichannel mapping system. It is apparent that at any instant of time, the field distribution over the nth incremental sampling area corresponds to that portion of the ξ, η plane which lies within the boundaries of the sampling increment. Hence it would appear that each filter output provides a continuous strip mapping of the radiating aperture as the mapping vehicle traverses the ξ, η plane. Continuing along this line of reasoning, it would follow that after suitable correction for the weighting factors, variation in R_n, etc., the combined output of the multichannel filter bank would result in a complete mapping of the aperture distribution in the ξ, η plane. Since the aperture distribution is continuously averaged over the dimensions of the parallelogram-shaped sampling increment, the accuracy of the measured distribution would of course depend upon the attainable resolution. Unfortunately other factors, which at this point are not apparent,
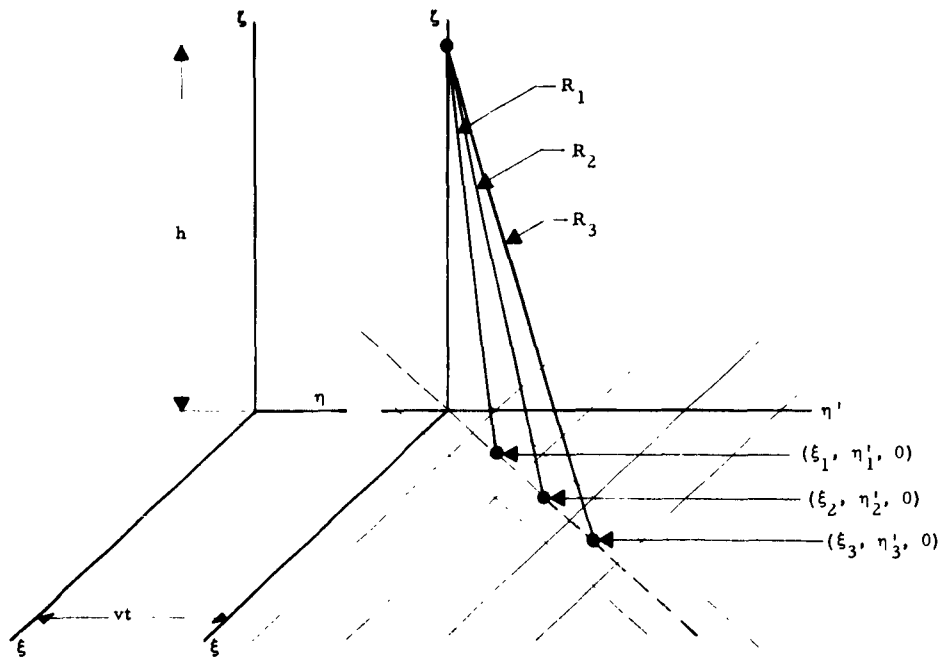
Figure 14. Sampling Areas of a Multichannel Mapping System

enter into the approach outlined above which greatly restrict the position of the sampling increment.

Equation (60) can be analyzed further on a qualitative basis by making the following simplifications: If the aperture distribution $F(\xi, \eta)$ is assumed to be essentially constant over the limits of integration, the term $F(\xi, \eta' + vt) W_1 W_2$ can be approximated at each instant of time by an average value $\overline{A}(t)$. This amounts to assuming a uniform distribution over the sampling increments which varies uniformly in intensity with t. Under this substitution it is possible to perform the integration of Equation (60); however, it is recognized that the tapering effect of the weighting functions W_1 and W_2 would tend to broaden the beam and decrease the sidelobe level of the resulting diffraction pattern. Under the assumptions stated, Equation (60) becomes

45

$$g_n(t) = C\,\overline{A}(t) \int_{\eta_n' - \frac{R_n}{kv}\,(2.78B)}^{\eta_n' + \frac{R_n}{kv}\,(2.78B)} \exp\left[jk\sin\theta(\eta' - \eta_n')\sin\phi\right]\,d\eta'$$

$$\bullet \int_{\eta'\tan a - 1.39\,\frac{R_n\lambda}{\pi L}\,\sec a}^{\eta'\tan a + 1.39\,\frac{R_n\lambda}{\pi L}\,\sec a} \exp\left[jk\sin\theta(\xi - \xi_n)\cos\phi\right]\,d\xi \qquad (61$$

where

$$C = \frac{j\,\exp\left[j\omega_o t - kR_n\right]}{4B\pi R_n^{\,2}} \qquad .$$

From Figure 11 the following relations are apparent

$$\sin\theta = \frac{\sqrt{\xi_n^2 + \eta_n'^{\,2}}}{R_n}$$

$$\sin\phi = -\frac{\eta_n'}{\sqrt{\xi_n^2 + \eta_n'^{\,2}}}$$

$$\cos\phi = -\frac{\xi_n}{\sqrt{\xi_n^2 + \eta_n'^{\,2}}} \qquad .$$

Under these conditions Equation (61) becomes

$$g_n(t) = C\,\bar{A}(t) \int_{\eta_n' - 2.78\,\frac{BR_n}{kv}}^{\eta_n' + 2.78\,\frac{BR_n}{kv}} \exp\left[-jk\,\frac{\eta_n'}{R_n}(\eta' - \eta_n')\right] d\eta'$$

$$\cdot \int_{\eta'\tan a - 1.39\,\frac{R_n\lambda}{\pi L}\sec a}^{\eta'\tan a + 1.39\,\frac{R_n\lambda}{\pi L}\sec a} \exp\left[-jk\,\frac{\xi_n}{R_n}(\xi - \xi_n)\right] d\xi \quad .$$

Performing the integration with respect to ξ produces

$$g_n(t) = C\,\bar{A}(t)\,\exp j\,\frac{k}{R_n}\left(\eta_n'^2 + \xi_n^2\right)\,2R_n\,\frac{\sin\left[\xi_n\left(1.39\,\frac{k\lambda}{\pi L}\sec a\right)\right]}{k\xi_n}$$

$$\cdot \int_{\eta_n' - 2.78\,\frac{BR_n}{kv}}^{\eta_n' + 2.78\,\frac{BR_n}{kv}} \exp\left[-j\,\frac{k\eta'}{R_n}(\eta_n' + \xi_n\tan a)\right] d\eta' \quad .$$

Integrating with respect to η' produces

$$g_n(t) = 4C\,\bar{A}(t)\,R_n^2\,\frac{\sin\left[\xi_n\left(1.39\,\frac{k\lambda}{\pi L}\sec a\right)\right]}{k\xi_n}\,\frac{\sin\left[2.78\,\frac{B}{v}(\eta_n' + \xi_n\tan a)\right]}{k(\eta_n' + \xi_n\tan a)}$$

47

which can be written as

$$g_n(t) = \frac{j \exp\left[j(\omega_o t - kR_n)\right]}{B\pi k^2} \ \overline{A}(t) \ \frac{\sin\left(\frac{2.78}{L}\sqrt{\eta_n'^2 + \xi_n^2}\ \tan a\right)}{\sqrt{\eta_n'^2 + \xi_n^2}\ \tan a}$$

$$\cdot \ \frac{\sin\left(\frac{2.78B}{v}\sqrt{\eta_n'^2 + \xi_n^2}\ \sec a\right)}{\sqrt{\eta_n'^2 + \xi_n^2}} \ . \tag{6}$$

The effect of η_n' and ξ_n on the received signal is immediately apparent from Equation (62). It is clear that the signal $g_n(t)$ is maximum for $\eta_n' = \xi_n = 0$ independent of angle a. It is also clear that as the radial distance

$$\rho = \sqrt{\eta_n'^2 + \xi_n^2}$$

increases, the received signal is attenuated by the two $\frac{\sin u}{u}$ terms through a series of nulls and relative maximums. To illustrate this effect, Equation (62) has been computed in the form of

$$f(\rho) = \left(\frac{\sin \gamma\rho}{\gamma\rho}\right)^2 \ . \tag{6}$$

This corresponds to the following parameter values

$$a = 37^\circ$$

$$\frac{1}{L} = \sqrt{2} \ \frac{B}{v}$$

where

B = 16 cycles

v = 1000 feet/second

L = 41.6 feet

γ = 0.056 .

Figure 15 is a curve of Equation (63) where the radius distance ρ is now measured along the 37° diagonal passing through the point (ξ_n, η'_n) and the point $(0, 0)$ in the ξ, η' plane. It can be concluded from these results that the sampling increment must be limited to a position directly under the probe. The signal from any other increment centered outside this region will be attenuated in a manner illustrated by Figure 15 which would clearly make the accuracy of the processed signal questionable and in some cases nonexistent. Under these restrictions, Equation (60) can be greatly simplified by performing the following substitutions. The center frequency of the sampling filter is taken to be the transmit frequency ω_o. No apparent advantage is gained by turning the sampling array, hence the skew angle a can be equal to zero. Finally, the coordinates ξ_n and η'_n are now $\xi_n = \xi_o = 0$ and $\eta'_n = \eta'_o = 0$. Under these substitutions, Equation (60) becomes

$$g_o(t) = \frac{j \exp\left[j(\omega_o t - kh)\right]}{B\pi h^2} \ Si\left[1.39\right] \ Si\left[1.39\right] \ \overline{A}(t) \tag{64}$$

49
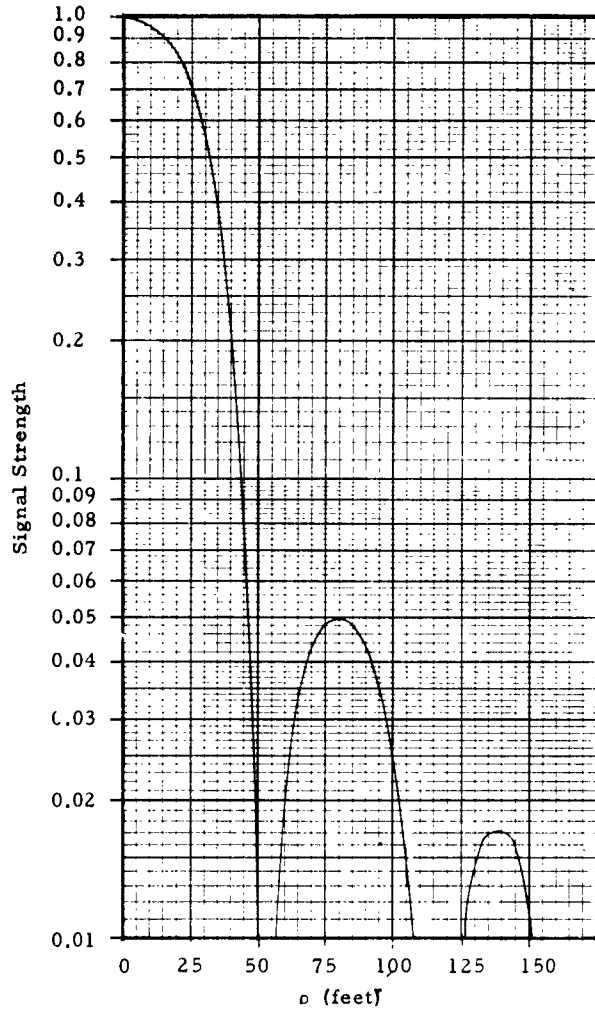
Figure 15. Signal Strength Versus Sampling Increment Displacement

where Si is the tabulated sine integral. Equation (64) reduces to

$$\overline{A}(t) = j\,2Bh^2 \exp\left[j(\omega_o t - kh)\right] g_o(t) \qquad (65)$$

where $\overline{A}(t)$ is the value of the aperture distribution, $F(\xi, \eta)$, averaged over a rectangular sampling increment centered at the point $\xi = 0$, $\eta = vt$. Figure 16 illustrates the geometry of this final configuration.

50
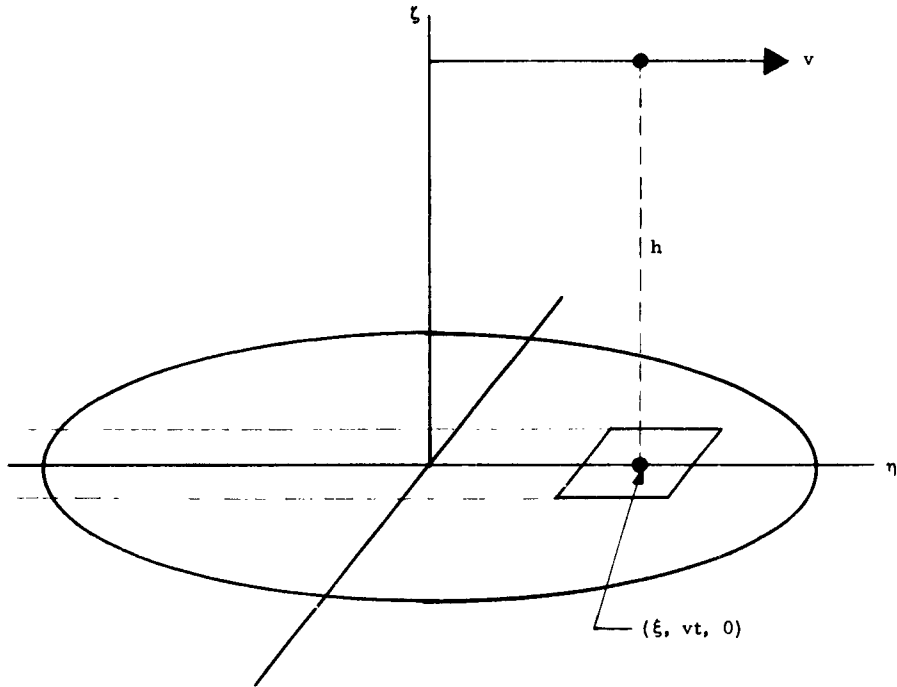
Figure 16. Principal Plane Mapping by Means of a Single
Incremental Sampling Area

While the feasibility of mapping the complete aperture in one flight
transit has proven to be unrealistic, it is apparent that conventional
plane cuts can be obtained by making several passes over the radiat-
ing aperture. The signal obtained from each transit would be a con-
tinuous mapping of the strip traced out by the sampling increment. As
was stated before, the accuracy of the measured distribution depends
mainly upon the size of the rectangular sampling increment; i.e., the
finer the resolution the more nearly the function $\overline{A}(t)$ represents the
distribution function at the point $(0, vt)$. Also, the limitations on the
position of the sampling increment have been shown to be a direct result
of the size of sampling increment.

This last observation can be further illustrated by a simple application of diffraction theory to the conditions of the isolated sampling increment. Consider a 1000-foot circular aperture which is to be measured by a vehicle traveling at an altitude of 1000 feet over the center of the radiating plane. Each isolated portion of the aperture can be thought of as exhibiting a diffraction pattern which is a function of the increment size. If the mapping vehicle is contained within the half power beamwidth of the most distant increment, it is clear that the beamwidth of the increment must be of the order of $2 \tan^{-1} \frac{500}{1000} = 53^{\circ}$. This corresponds to a radiating aperture with maximum dimensions of less than a wavelength.

Several factors affect the resolving power of the sampling system. Increasing the altitude of the probe decreases the off-axis angle, but this effect is nullified by the increased area subtended by the sampling antenna beamwidth. Increasing the velocity of the sampling vehicle would produce a greater Doppler shift and hence a greater filter resolution for a given bandwidth, but this occurs in one dimension only, and it has been shown that the ratio $\frac{v}{B}$ is subject to a maximum critical value.

One possible approach to this problem is synthetic aperture type signal processing. This is analyzed in some detail in the following section.

B. Synthetic Aperture Processing

One possible approach to obtaining greater sampling resolution is the application of synthetic aperture type processing to the signal received from the sampling area. In recent years this system has been developed in connection with ground-mapping radar to such a degree that azimuth resolutions (independent of range and wavelength) of the order of a few feet are obtainable. Since most of the material available on this subject is still classified, only a brief discussion will be presented here.

In ground-mapping radar applications, the transmitting antenna used in a typical synthetic aperture system is "side looking", relatively narrow beam, and of physical dimensions compatible with airborne requirements. Range resolution is obtained by conventional pulsing techniques while azimuth resolution is obtained by recording a series of returns from each point target and then processing the recorded data such that the physical antenna becomes an element of a large synthetic array. The number of elements in the array is equal to the number of pulses recorded from each point target. Figure 17 illustrates the geometry of a typical airborne ground-mapping radar.

It is apparent that the number of return pulses and hence the length of the synthetic array is a function of the pulse repetition rate and the length of time that the point target at P lies within the specular area of the antenna beam. Hence, flight velocity and beamwidth are also factors governing the length of the synthetic array. Broadly speaking, the length of the synthetic array will be comparable to the longitudinal dimension of the specular trace and will have the conventional resolving power of a physical antenna of that length.
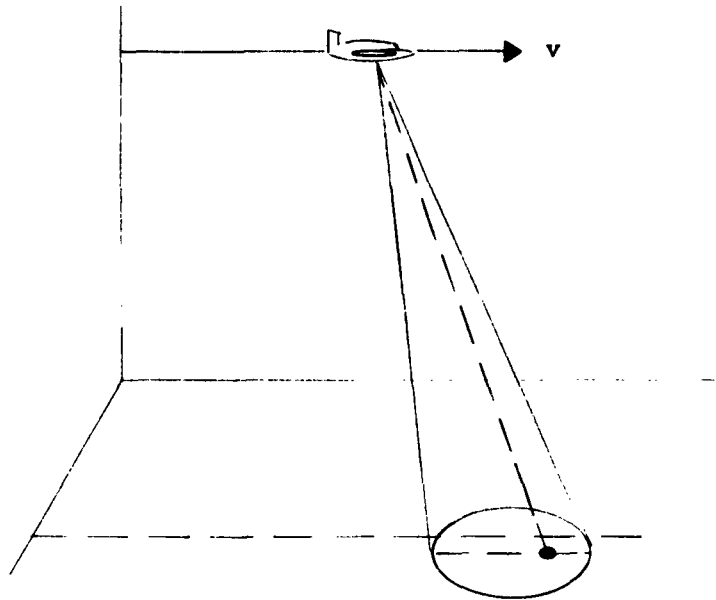
Figure 17.   Geometry of a Side-Looking Synthetic Aperture
Processing Ground-Mapping Radar

In developing a suitable processing system it can be assumed
that the coherently pulsed signal is continuous.   Under this condition,
the returned signal from a particular point target is continuous with its
frequency modified by a time and range dependent Doppler effect.   There-
fore each point target generates its own continuous and unique Doppler
history as it passes through the specular trace of the physical antenna.
For example, in the case of a broadside looking antenna (i.e., main
beam normal to the direction of flight), the frequency of the received
signal changes from a higher to a lower value than that of the transmitted
frequency as the target enters and leaves the specular trace.   Further,
when the target is exactly at the broadside position, the transmit and
receive frequencies are the same.   This configuration has been used in
connection with a coherent reference oscillator and a pulse integration

system in which the complete return from each target is compressed about the "zero beat" point produced by beating the time-varying return signal against the stable local oscillator.[6] The zero beat point and hence the center of the compressed return signal serves to identify the azimuthal position of the point target with respect to the mapping vehicle.

Processing techniques have been developed using vector addition, cross correlation, and filtering approaches. However, in a recent publication it has been shown that these three approaches are equivalent,[7] hence in analyzing a particular aspect of a given system, the most applicable approach should be used.

Although grossly over-simplified, the foregoing discussion contains sufficient information for deducing certain conclusions regarding the mapping of radiating apertures via synthetic aperture processing techniques. As in any pulsed radar, the operation of a synthetic aperture system consists of periods of transmission, during which time wave trains of finite length are launched towards the target area, followed by periods of reception during which time the reflected portions of the transmitted wave are received. Hence during the period of reception, the target area is analogous to a two-dimensional array whose elements consist of all the point targets which lie within the specular trace of the physical antenna. Therefore, it would appear that the transition from ground mapping to aperture mapping is a logical and straightforward step. However, further investigation into the nature of the quasi-point sources on which the analyses of the two "radiating apertures" are based, brings out complications which appear to make the two systems incompatible.

Continuing the analysis of the specular trace on the basis of

a two-dimensional array, it is apparent that the energy distribution on

each element (i.e., point target) is dependent upon the reflection coef-

ficient and the position of the point target with respect to the illuminating

and receiving antenna. Hence the target area as an array is made up of

an arbitrary number of elements with distributions essentially random

in both magnitude and phase. Clearly this is a necessary condition for

the operation of synthetic aperture type processing (i.e., each target

must have a unique Doppler history during its passage through the spec-

ular trace). For example, consider a target area made up of a large

number of identical, closely-spaced point targets. Under these condi-

tions the reflected energy is no longer made up of discrete incoherent

wavelets. Instead, as the separation between targets is decreased, the

reflected wave trains from adjacent targets begin to overlap in a well-

defined manner. The result is threefold.

1.   The overlapping of the returned wave trains makes pulse
      ranging impossible.

2.   The Doppler frequency histories of adjacent targets begin
      to "look" alike.

3.   Reinforcement and cancellation resulting from the coher-
      ence of the reflected wavelets produce the usual lobed
      pattern associated with any aperture which is illuminated
      in an orderly manner.

Any of these three effects would make the synthetic processing system

inapplicable. However, for an actual illuminated aperture, the third

effect as discussed in the preceding section is probably the most deci-

sive. Hence, it appears that the coherent nature of the quasi-point dis-

tribution of a radiating aperture is incompatible with the requirements

of synthetic aperture processing.

Having established the limitations of the foregoing analysis as regards the number and position of sampling areas, any further discussion will be restricted to the conditions of the area directly under the probe. In general, the distribution over an isolated portion of an arbitrarily illuminated aperture will be nonlinear and asymmetrical in both amplitude and phase. The added weighting effect of the filter function and sampling array pattern produces an aperture distribution that is extremely complex. Fortunately, only a qualitative analysis is needed and this can be accomplished with a sufficient degree of accuracy from line source considerations. As reported by R. C. Spencer,[8] the diffraction field of a line source can be analyzed in terms of the line distribution moments. For an arbitrary distribution, $f(x)$, the normalized diffraction integral is,

$$g(u) = \int_{-1}^{1} f(x) \, \exp\left(j \, \frac{\pi a x}{\lambda} \, \sin \theta\right) \, \exp\left(-j\beta x\right) \, dx \qquad ($$

where

$$g(u) = \text{Franhofer diffraction field}$$

$$f(x) = \text{amplitude distribution}$$

$$a = \text{length of the line source}$$

$$\lambda = \text{wavelength}$$

$$\exp\left(-j\beta x\right) = \text{linear phase deviation} \, .$$

Equation (66) can be expanded into its infinite series with the result

$$g(u) = \mu_o - \frac{\mu_2}{2!} u^2 + \frac{\mu_4}{4!} u^4 - \ldots + j\left[\mu_1 u - \frac{\mu_3}{3!} u^3 + \frac{\mu_5}{5!} u^5 - \ldots\right]$$

(6

where

$$u = \frac{\pi a}{\lambda} \sin\theta - \beta$$

$$\mu_k = \int_{-1}^{1} x^k f(x) \, dx \quad .$$

μ_k is referred to as the kth moment of $f(x)$. The power pattern $P(u)$ follows from the sum of the squares of the real and imaginary series of Equation (67),

$$P(u) = \mu_o^2 - (\mu_o \mu_2 - \mu_1)^2 u^2 + \left(\frac{\mu_o \mu_4}{12} - \frac{\mu_1 \mu_3}{3} + \frac{\mu_2^2}{4}\right) u^4 - \ldots$$

((

Multiplicative constants have been deleted in Equations (66) through (68).

Several important factors are immediately apparent from Equations (67) and (68). First, it follows from the definition of μ_k that even and odd distribution functions produce respectively, pure real and pure imaginary diffraction field series, which are again respectively even and odd functions of the variable u. In the general case, both real and imaginary components are present, however. Equation (68) indicates that the power pattern is still symmetric about $u = 0$ and is a

58

principal maximum there. Thus, the only asymmetry resulting from an arbitrary amplitude distribution is the sign reversal in the imaginary component of the field intensity which accompanies the sign reversal of the u variable. The effect of the linear phase distribution can be seen from the relation[4]

$$u = \frac{\pi a}{\lambda} \sin \theta - \beta \quad .$$

For $u = 0$, $\frac{\pi a}{\lambda} \sin \theta = \beta$, hence the principal maximum or direction of the main lobe is skewed by an angle β.

From these results, the following assumptions can be made regarding large apertures with arbitrary amplitude distributions and moderate but continuous phase variations. A small isolated area centered about a point in the plane of the aperture exhibits a symmetrical power pattern with the principal lobe axis normal to the phase front at the point. The on-axis field intensity is proportional to the zero distribution moment which is simply the aperture distribution integrated over the incremental sampling area, and the extraction of relative phase and amplitude from a signal of this type can be performed in a conventional manner.

V.   ERROR ANALYSIS

The errors associated with performing pattern measurements with the Transverse Doppler Pattern Measurement Technique fall logically into two categories: one includes the inaccuracies which are inherent in the technique; the other consists of those errors which arise from deviations in the assumed values of system parameters.

The former are, in general, functions of the system aperture resolution, where the resolution is dependent on the composite parameter $\frac{kva}{2Bh}$ in the longitudinal dimension, and on the directional characteristics of the sampling probe in the transverse dimension. Since the resolution increment is of finite dimension and the measuring technique involves essentially an averaging of the response received from the increment, the ability of the system to resolve local variations from the average is limited. In the case of the line source, the response is averaged only over the longitudinal dimension of the sampling increment. For a two-dimensional aperture, sampled by an omnidirectional probe, the response is averaged over the transverse dimension of the aperture as well, and the filtered signal is weighted by both the aperture distribution in the transverse direction and the transverse extent of the aperture.

However, if a linear array is used for the sampling antenna, the transverse dimension over which the signal is averaged is reduced to a length proportional to the beamwidth of the linear array. Under this condition, the weighting effect of the aperture distribution in the transverse dimension is lessened; however, the effect of the pattern factor of the linear array must be accounted for in the final result.

To determine the effect of errors attributable to system limitations in the measurement of the aperture distribution, far field patterns were computed from the "measured" aperture distributions of a line source 500λ in length for several values of system parameters and aperture distributions. These cases are plotted and discussed on pages 41 through 57 of Scientific Report No. 1.[5] In general, the patterns computed from the measured distributions are in good agreement with the exact patterns in the main beam region, but are optimistic compared to the exact pattern outside of this region.

Errors which are the result of variations in system parameters, e.g., height, velocity, operating frequency, etc., during the measurement interval are somewhat more difficult to analyze quantitatively. However, what qualitative effects these deviations will have are readily deduced from a consideration of Equation (15). Basically the system parameters which may be expected to vary appear in three places in this expression: in the amplitude factor, in the phase factor, and in the resolution of the sampling function.

Since the time required for taking the measurement data (or aperture fly-by time) will be of the order of two seconds, variations in the transmitted frequency during this time will be very small, perhaps of the order of one part in 10^8 at UHF.[9] The frequency dependence appears as the parameter $k \left(\frac{2\pi}{\lambda} \right)$ in all three factors of the equation, and since $\Delta k = k \frac{\Delta f}{f}$, variations of this order in frequency have little effect on system accuracy. Even in the phase factor a variation in k of approximately two parts in 10^3 are required for π radians of phase change with h = 1500 feet. An additional condition on frequency stability has been assumed in the filter function of Equation (10), i.e.

$$H_2(\omega) = \frac{\sin\left(\dfrac{\omega - \omega_o}{2B}\right)}{\omega - \omega_o}$$

(1

However, since the band of frequencies about ω_o, is essentially contin-
uous (except near the ends of the aperture) because of the Doppler con-
tributions, a moderate change in ω_o corresponds to sampling a strip of
the aperture which is located either slightly ahead or slightly behind the
probe vehicle rather than directly beneath it. For example, at a velocity
of 880 ft/sec, a variation in frequency of one part in 10^8 causes an angu-
lar shift of the sampling region of approximately one percent.

Probe height, h, appears in both the phase factor and the argu-
ment of the sampling function. In the sampling function, the effect of
changes in h appear as variations in the resolution of the aperture. As
can be seen from Figures 5b, 20, and 21 of Scientific Report No. 1,[5]
changes in the composite parameter, $K = kva/2Bh$, over a large range
(2 to 1) have a relatively small effect on the accuracy of the aperture
distribution measurement and the corresponding far field pattern once a
certain minimum value of the parameter K is exceeded. In view of this
fact, it appears that small changes in the values of any of the individual
factors of K will not limit the accuracy of the measurement technique.

The height, h, appears also in the phase factor. The phase may
be written as

$$k\sqrt{h^2 + \xi^2} = kh\sqrt{1 + \left(\frac{\xi}{h}\right)^2}$$

(69

and varies essentially as kh. Since h is of the order of one to two thousand feet, very small changes in h percentage-wise can cause the phase to shift appreciably. For a linear change in h, the effect is that of a linear phase shift across the aperture and can cause difficulty. Therefore, it appears that it will be necessary to limit the variation in h to the order of a wavelength during the measurement period. However, in the event that large flight path deviations, in terms of wavelength, are unavoidable, it is possible to detect such deviations by means of a Doppler and/or inertial stabilization system such as those used in conjunction with ground-mapping radars. Such a system provides continuous monitoring of pitch, roll, altitude, and velocity; hence the output signal can be used to compensate for any deviations in flight path by electronically scanning the sampling antenna, adjusting the filter frequencies, and by varying the phase of the received signal in accordance with incremental changes in altitude.

As was pointed out in Section III, the presence of a large linear phase distribution in the radiating aperture necessitates a modification of the mapping technique. Fortunately the solution to this problem is straightforward and is contained in the general expression for the Doppler frequency shift.

Referring to the geometry of Figure 1b, the frequency of the signal received from a point in the ξ, η plane by the probe at P is given by

$$\omega_d = \omega_o + \frac{\omega_o}{c} \frac{dr}{dt} \tag{7}$$

where c is the velocity of light and the term

$$\frac{\omega_o}{c} \frac{dr}{dt}$$

is the Doppler frequency shift.

It has been shown that the radial distance, r, connecting P and the point (ξ, η) is of the form

$$r = \sqrt{(vt - \eta)^2 + h^2 + \xi^2} \quad .$$

(7

Therefore, the Doppler frequency equation is,

$$\omega_d = \omega_o + \frac{\omega_o v(vt - \eta)}{c\sqrt{(vt - \eta)^2 + h^2 + \xi^2}} \quad .$$

(7

It should be mentioned that the proper sign has been chosen for the radical of Equation (72) so that the Doppler shift is positive for $\eta > 0$ and negative for $\eta < 0$.

For constant Doppler frequencies $\omega_d = \omega_i$, $i = 1, 2, 3, \dots$, Equation (72) becomes

$$(\omega_i - \omega_o)^2 = \frac{\omega_o^2 v^2 (vt - \eta)^2}{c^2 \left[(vt - \eta)^2 + h^2 + \xi^2\right]}$$

(7

which reduces to

$$(vt - \eta)^2 \left[\frac{\omega_o^2 v^2}{c^2 (\omega_i - \omega_o)^2} - 1 \right] - \xi^2 = h^2 \quad . \tag{74}$$

For

$$\frac{\omega_o^2 v^2}{c^2 (\omega_i - \omega_o)^2} > 1 \quad ,$$

as is the case here, Equation (74) represents a family of hyperbolas with foci shifted along the η axis by the linear function of time, vt.

As was stated earlier, the physical significance of this is that there is associated with a bank of filters at the probe P, a grid of hyperbolic contours in the ξ, η plane which travels in the same direction and at the same velocity as the probe.

The effect of a large linear phase deviation will now be considered. The geometry of Figure 18 corresponds to that of Figure 1b with the exception of the tilted plane W which represents a wavefront emanating from an aperture in the ξ, η plane which has been electronically scanned through an angle θ in the ζ, η plane. From the geometry, the slant range r connecting the probe at P with a general point in W is

$$r = \sqrt{\xi^2 + (\eta - vt)^2 + (h - \zeta)^2}$$
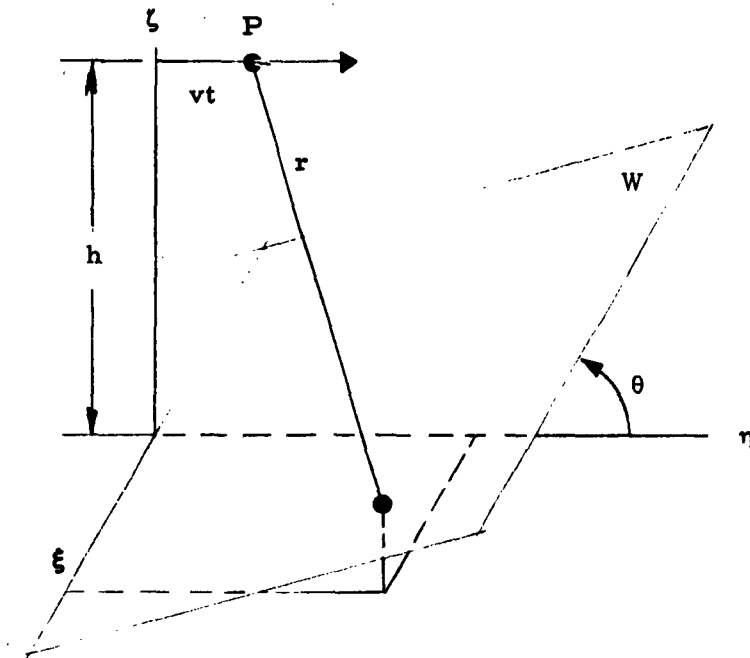
Figure 18.   Plane Wavefront of an Electronically-Scanned Aperture

where

$$\frac{\zeta}{\eta} = \tan \theta \quad .$$

Therefore

$$\frac{dr}{dt} = \frac{-v(\eta - vt)}{\sqrt{\xi^2 + (\eta - vt)^2 + (h - \eta \tan \theta)^2}} \quad .$$

Hence the frequency of the signal at P is

$$\omega_d = \omega_o + \frac{\omega_o v(\eta - vt)}{c\sqrt{\xi^2 + (\eta - vt)^2 + (h - \eta \tan \theta)^2}} \quad .$$

Equation (75) differs from Equation (72) in that the term $(h - \eta \tan \theta)^2$ appears under the radical instead of h^2. Because of this, Equation (72) does not represent a traveling grid of fixed contours such as was developed from Equation (72). By following the procedure used to obtain Equation (74), it can be shown that the resulting traveling grid is made up of contours in the ξ, η plane which change shape as a function of time. However, one important exception exists which is more readily seen if the ξ, η plane is rotated into the plane of the phase front. Figure 19 illustrates the results of this rotation. The expression for r is now

$$r = \sqrt{\xi^2 + (\eta - vt \cos \theta)^2 + (h - vt \sin \theta)^2} \quad .$$
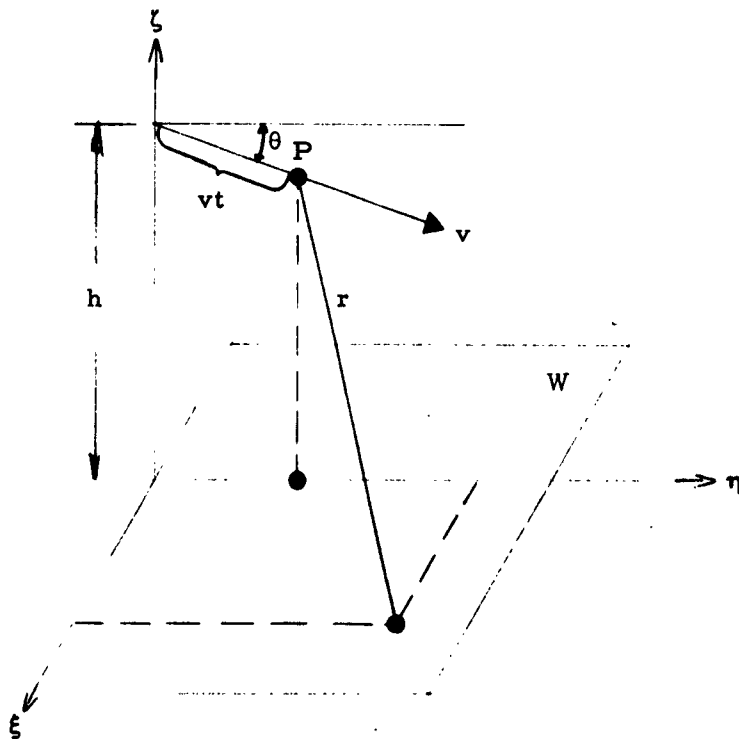
Figure 19. Plane Wavefront of an Electronically-Scanned
Aperture Rotated into the ξ, η Plane

$$\omega_d = \omega_o + \frac{\omega_o\left[(\eta - vt\cos\theta)\,v\cos\theta + (h + vt\sin\theta)\,v\sin\theta\right]}{c\sqrt{\xi^2 + (\eta - vt\cos\theta)^2 + (h - vt\sin\theta)^2}} \quad . \tag{76}$$

It can be seen from Equation (76) that the frequency of the signal received from the point directly under P is independent of t for if the ξ, η coordinates of P (i.e., $\xi = 0$, $\eta = vt\cos\theta$) are substituted into the equation, the result is

$$\omega_d = \omega_o + \frac{\omega_o(h - vt\sin\theta)\,v\sin\theta}{c(h - vt\sin\theta)}$$

or

$$\omega_d = \omega_o + \frac{\omega_o}{c}\,v\sin\theta \quad . \tag{77}$$

Hence it can be concluded that if the slant range r is at all times normal to the wavefront, the frequency of the signal received from the incremental area will be constant and will differ from the fundamental frequency ω_o by an amount proportional to the component of velocity in the direction of r. Referring to Figure 20 it can be seen that this amounts to shifting the slant range r ahead of the vertical by an amount equal to the scan angle θ.

An alternate approach to this analysis is the consideration of the time rate of change of phase produced by the motion of the probe with respect to a constant phase front. Referring to Figure 20, if θ is fixed and

r is extended to point P' on the η axis, it is clear that the length PP' does not change as P traverses a path parallel to the η axis. Hence the Doppler shift is zero, however; the change in phase which occurs at the moving point P' is not zero and can be expressed as

$$\frac{d\phi}{dt} = \frac{d}{dt}\left[\frac{2\pi}{\lambda_o} \eta \tan \theta\right]$$

where $\left(\dfrac{2\pi}{\lambda_o} \eta \tan \theta\right)$ is the linear phase distribution in radians per unit length. From the geometry of Figure 20,
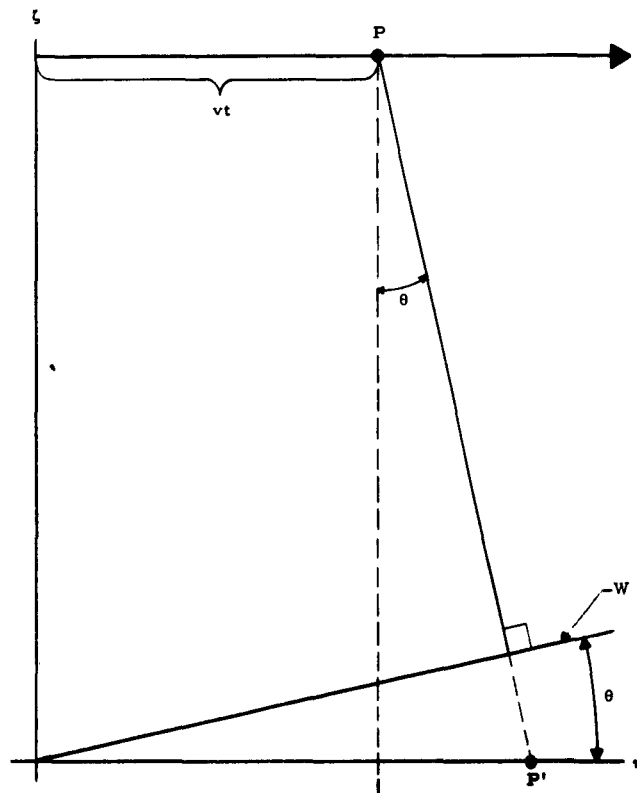

Figure 20. Position of Slant Range r for a Constant Doppler Frequency Shift

$$\eta = h \tan \theta + vt \quad .$$

Therefore

$$\frac{d\phi}{dt} = \frac{2\pi}{\lambda_o} \tan \theta \frac{d}{dt}\left[h \tan \theta + vt\right]$$

$$= \frac{2\pi v}{\lambda_o} \tan \theta$$

which in terms of frequency reduces to

$$\omega = \omega_o \frac{v}{c} \tan \theta \quad . \tag{7}$$

Equation (78) is equivalent to the last term of Equation (77), for in both equations the frequency shift is given by the product of the component of velocity normal to the wavefront and the factor $\frac{\omega_o}{c}$.

Hence, it may again be concluded that the frequency of the signal received from an incremental area centered about the point P' is constant provided that r is normal to the wavefront.

VI. EXPERIMENTAL DEMONSTRATION

An analytic investigation of this type should be accompanied by an experimental program designed to verify the mathematical description of the system and to establish the practical feasibility of the approach. Generally, this experimental program can be of two types. One is a program carried out in the laboratory, where modeling or scaling of the physical components is done to achieve convenient values of size, frequency, etc. The other type is an actual field measurement program with a minimum or breadboard system using conveniently available existing facilities. Application of each of these avenues of approach to an experimental demonstration of the Transverse Doppler Pattern Measurement Technique is discussed below, with emphasis on performing an adequate demonstration with a modest amount of time and effort.

As indicated in the material presented above, this technique is most readily applied to linear arrays or rectangular apertures with separable distributions. Accordingly, the experimental programs discussed assume linear arrays as the radiating structures. Extension to rectangular arrays is, of course, straightforward.

A.   A Laboratory Demonstration

Since this program is concerned with the measurement of the patterns of large antennas (large both physically and electrically), modeling or scaling of the radiating structure and the probe vehicle is required for work in the laboratory. Reduction of both the physical and electrical sizes of these structures may be accomplished by scaling in frequency. If one somewhat arbitrarily chooses 100λ as a typical aperture.

electrical length and 10 feet as a practical length for experimentation in the laboratory, these sizes can be obtained at a frequency of 9830 Mc. Using Figure 3 (page 16), for ka = 628.4, a = 2, and a linear resolution corresponding to N = 10, kv/B = 17.6. With B = 30 cps, v = 8.4 ft/sec. From Figure 4, kh = 197, giving h = 3.14 feet. Summarizing, the system parameters then are:

$$L = 100\lambda = 10 \text{ feet}$$

$$f = 9830 \text{ Mc}$$

$$h = 3.14 \text{ feet}$$

$$v = 8.4 \text{ ft/sec}$$

$$B = 30 \text{ cps}$$

$$N = 10 .$$

A quite compact arrangement may be designed with these parameters. The main problem is, of course, that any reasonably-sized probe vehicle is too small to carry the required signal processing system. Therefore, a means of transferring the signal received at the probe antenna to a stationary signal processing system must be provided. Perhaps the simplest way is to transfer the signal with a coaxial transmission line of sufficient length to allow the probe vehicle to move freely over its entire path.

A schematic of this laboratory system and a conceptual drawing of its layout are shown in Figures 21 and 22. In Figure 21 the linear array is indicated at the left with the movable probe antenna shown to the right of it. A portion of the transmitter signal is used as the local
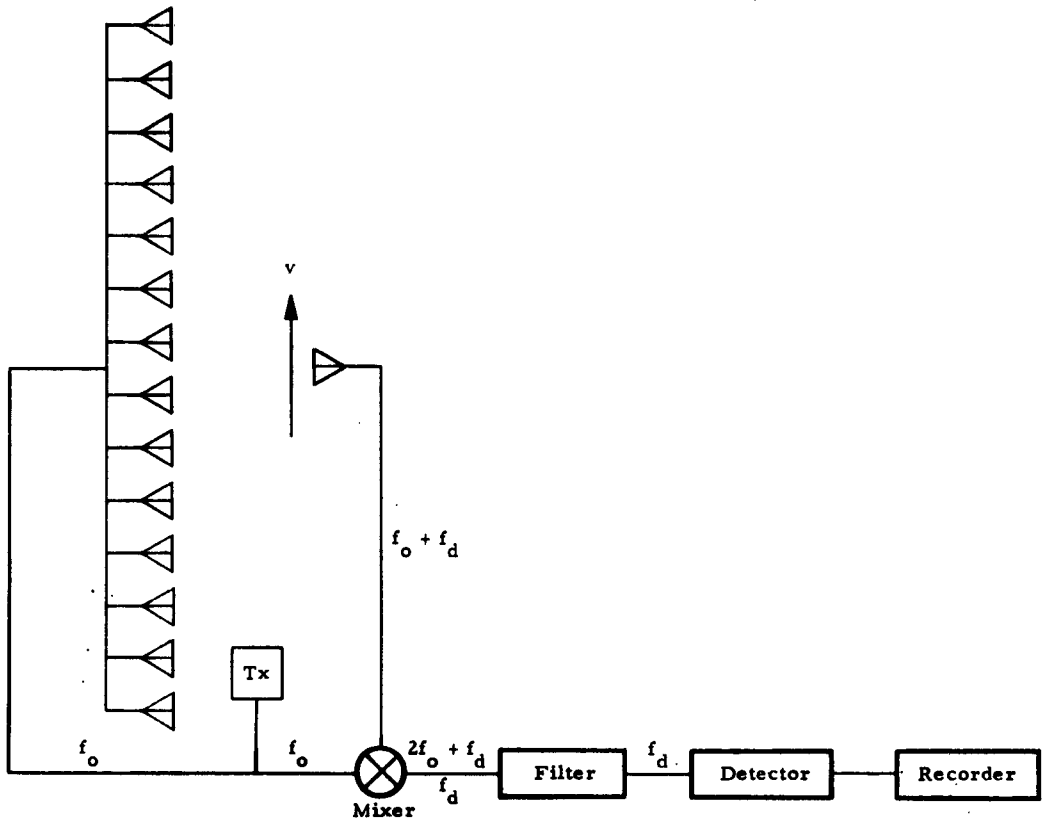
Figure 21. Schematic of Laboratory Experiment

oscillator signal and mixed with the signal received by the probe antenna
to form a homodyne (or 0 IF) receiving system. The mixer is followed
by a low-pass filter to provide the resolution on the aperture, phase, and
amplitude detector, and a dual trace recorder.

By using a portion of the transmitter power as the local
oscillator signal, good audio frequency stability can be obtained without
requiring excessive stability in the RF signal. Narrowband filtering of
the Doppler component can then be accomplished without difficulty.
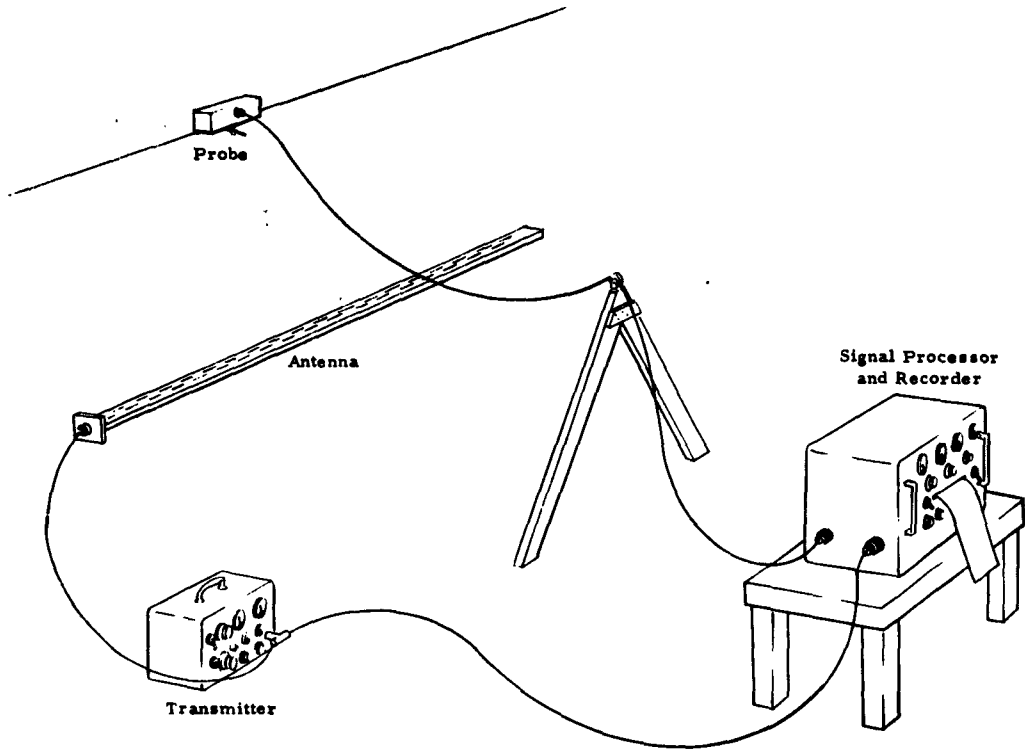
Figure 22. Conceptual Drawing of the Laboratory Experimental System

Figure 22 is an artist's conception of the experimental setup.
The antenna whose far field pattern is to be measured consists of a 100λ
X-band waveguide linear array. Suspended above the array on a nylon
line is a small carriage for supporting the probe antenna. Since the aper-
ture length is 10 feet, a probe path length of approximately 20 to 30 feet
will be required to adequately simulate actual full scale measurement
conditions. A high speed synchronous electric motor with its shaft speed
reduced in a gear train supplies the motive power for the carriage. The
motor is located at one end of the probe carriage path and draws the car-
riage toward itself with a nylon cord. A second nylon cord, attached to
the opposite end of the carriage, leads to a device which provides a small

constant tension opposing the motion of the carriage. This insures that the probe velocity will remain essentially constant over the major portion of its travel. An automatic limit switch is provided to disengage the motor as the extremity of the carriage travel is approached. The probe antenna is an X-band, half-wavelength dipole suspended from the carriage. The RF signal received by the probe antenna is fed through a length of flexible miniature shielded coaxial transmission line to the signal processing network, then detected and recorded. The recorded trace is a plot of received signal versus time and corresponds to the aperture distribution. Both phase and amplitude detection must be performed in order to determine the distribution. The far field characteristics are then determined by integration of the aperture distribution.

Evaluation of the system's performance in measuring various aperture distributions may be made by measuring the aperture distributions of the antennas and comparing the far field patterns computed from the measured aperture distributions with the actual patterns measured by conventional means in the far fields of the antennas. Fabrication of individual slot waveguide arrays for a variety of amplitude and phase distributions is required to obtain the test arrays.

An alternate arrangement of the experimental setup is shown in Figure 23. Here the probe path is vertical rather than horizontal and some of the difficulty in maintaining a constant distance between the probe and the aperture is alleviated.
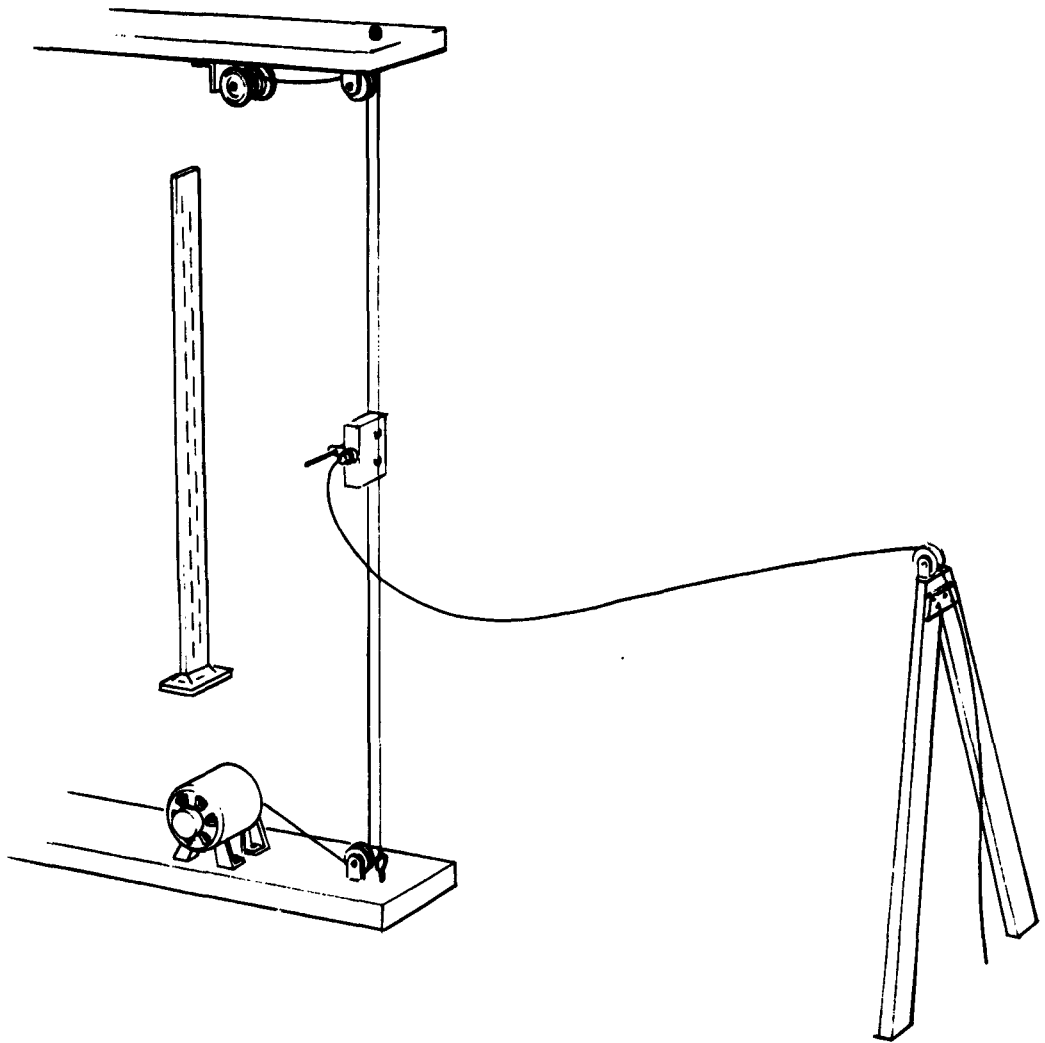
Figure 23.   Conceptual Drawing of Alternate Laboratory Experimental
System

B. Field Demonstration

Because of the availability of several large antennas located throughout the country, it is possible that a full scale demonstration might be preferable to the scaled experiment outlined above. Certainly in the final analysis, a full scale program must be carried out; hence if the laboratory experiment can be avoided, much time and expense will also be avoided.

The apparent advantages of a full scale approach then are twofold:

1. Elimination of the design and fabrication of a transmitting antenna.

2. More realistic results.

For example, consider the long linear array located near Archer City, Texas (part of the U.S. Navy's space surveillance system); this array has a maximum linear dimension of one mile. At the frequency of operation, this corresponds to a length of the order of 1000 wavelengths. Typical parameters for an antenna of this size are:

$$a = 2$$

$$N = 60$$

$$V = 840 \text{ ft/sec}$$

$$B = 30 \text{ cps}$$

$$h = 1190 \text{ feet}$$

These values have been computed from the curves of Figures 3 and 4.

Using these parameters, the experimental procedure differs from that of the laboratory technique in essentially two ways:

1. A portion of the transmitter output can no longer be used as a local oscillator signal.

2. Variations in probe path, both direction and velocity, must be considered.

Of the former, no great difficulty is encountered since local oscillators with frequency stability factors of the order of one part in 10^8 are well within the state-of-the-art.

Concerning probe path variations, as has been stated in Section IV. B, errors of this type can be detected and compensated for by means of a suitable inertial system; however, since the fly-by time is low, it is felt that these effects can be ignored in the initial experimental investigation.

It should be noted that all data processing and recording equipment can be carried by the mapping vehicle, where the stable local oscillator frequency is determined by the desired off-set from the ground transmitter frequency.

Since the array considered here is a discrete element array, the aperture distribution is available by actual element measurement. Hence the antenna provides an accurate experimental standard. Figure 24 illustrates the mapping vehicle, the test array, and the data processing system. The sampling probe is a single element which provides large angular coverage. The received signal is mixed with a signal equal in frequency to the ground-stationed transmitter, and the output
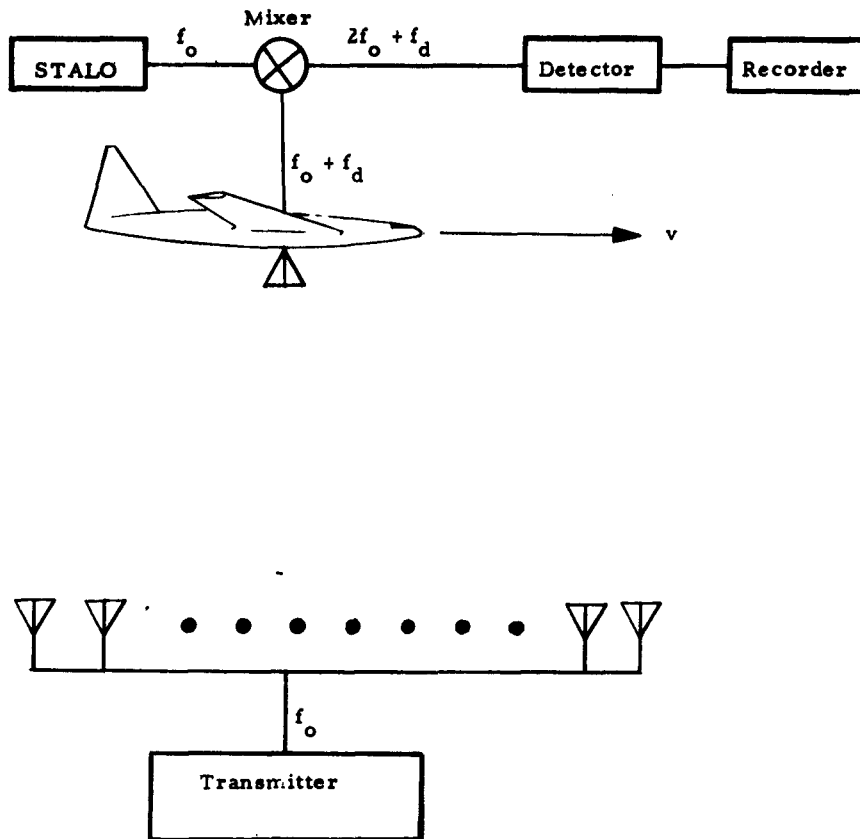
Figure 24. Schematic of Experimental Field Demonstration

of the mixer is then passed through a low pass filter. The output of the filter then contains the desired information concerning the average phase and amplitude of the energy radiating from the sampling strip.

It is felt that data obtained in an experiment of this type would provide, at a nominal expense, much information on the feasibility, limits, and accuracy of Transverse Doppler Pattern Measurements.

VII. SUMMARY AND CONCLUSIONS

A mathematical description of the Transverse Doppler Pattern Measurement Technique has been derived on the basis of the scalar diffraction equation. In the initial phase the effect of Doppler frequency filtering was analyzed and the results of this analysis were applied to specific and one- and two-dimensional apertures. The data computed from this application have established certain limitations as to the versatility of a Doppler filter sampling system. Specifically, it has been shown that this technique provides a sampling resolution in one dimension only and is therefore most applicable to linear arrays and rectangular apertures with separable distribution.

In an attempt to develop a technique suitable for more general apertures and distributions, a second analysis was performed which included the effect of a linear array sampling antenna. Because of the additional resolving power of the directional sampling antenna, it was possible to derive a sampling function which isolated, within the boundaries of an arbitrary two-dimensional aperture, a rectangular sampling area of comparatively small dimensions.

In an attempt to extend this approach, the effect of multichannel processing was examined in which the radiating aperture was broken up into a series of incremental areas by means of a multichannel Doppler filter bank. It was found that while this concept is mathematically feasible, limitations are again encountered because of the directional dependency of the signal received from each sampling increment. Since this directional dependency is a function of sampling increment size, an attempt to increase the sampling system resolution was made by utilizing

80

the concept of synthetic aperture processing. Here again the coherence of the quasi-point sources which make up the aperture distribution proved to be detrimental and it was shown that synthetic aperture processing is not applicable to the Transverse Doppler Pattern Measurement Technique.

It has been concluded that the technique developed, while in some respects limited, are suitable for measuring with good accuracy a variety of large one- and two-dimensional arrays. The extent of the accuracy is of course dependent upon many factors and has been discussed in some detail in the Error Analysis section of the report.

Specifically, it is felt that long linear arrays and two-dimensional arrays with separable distributions can be mapped with a minimum of equipment and expense. Hence, two experimental procedures have been outlined cn this basis which are designed to prove the feasibility of the analytic results.

However, it is emphasized that while the possibility of mapping an entire aperture in one probe transit does not appear to be feasible, a technique has been developed which provides for the principal plane distribution mapping of any aperture.

In the case of a one-dimensional array, the result is of course the linear distribution. For a two-dimensional array with separable distribution, sampling by means of a simple probe produces a mapping of the aperture distribution in the direction of probe transit which is weighted by the transverse aperture distribution. In this case, a second orthogonal cut is needed in order to separate the mutual weighting effects of the distribution functions. If a linear array sampling probe is used,

principal plane aperture distribution cuts can be obtained from any type of radiating aperture. It has been shown that even the large phase deviations associated with electronically-scanned apertures present no problem.

Hence, it is apparent that the Transverse Doppler Pattern Measurement Technique is feasible and has great potential in the expanding field of large aperture antennas. It is felt that the next logical step is the development of an operational system. As outlined in Section VI, a scaled laboratory experiment or a rudimental field measurement would provide much information concerning the actual hardware needed to detect, process, and record the sampling system data. Having accomplished this, it remains to refine the system resulting in a reliable and accurate system for obtaining the radiation characteristics of large aperture antennas from measurements in the near field.

APPENDIX A

A formulation which appears to somewhat simplify the computational difficulties of Equation (32) may be obtained by retaining the aperture coordinates in polar form. Under these conditions, the equation corresponding to Equation (8) is

$$S_y(t) = \frac{jk}{(2\pi)^2} \int_0^{2\pi} d\psi \int_0^a \rho F(\rho)\, d\rho \int_{-\infty}^{\infty} H(\omega) \exp(j\omega t)\, d\omega$$

$$\cdot \int_{-\infty}^{\infty} \frac{\exp\left\{-jk\left[(vt' - \rho \sin\psi)^2 + h^2 + \rho^2 \cos^2\psi\right]^{1/2} - j(\omega - \omega_o)\, t'\right\}}{\left[(vt' - \rho \sin\psi)^2 + h^2 + \rho^2 \cos^2\psi\right]^{1/2}}\, dt'$$

$$= \frac{jk}{(2\pi)^2} \int_0^{2\pi} d\psi \int_0^a \rho F(\rho)\, d\rho \int_{-\infty}^{\infty} H(\omega) \exp\left\{j\left[\omega t - \left(\frac{\omega - \omega_o}{v}\right)\rho \sin\psi\right]\right\} d\omega$$

$$\cdot \int_{-\infty}^{\infty} \frac{\exp\left\{-jk\left[\frac{\omega - \omega_o}{kv}(vt' - \rho\sin\psi) + \sqrt{(vt' - \rho\sin\psi)^2 + h^2 + \rho^2\cos^2\psi}\right]\right\}}{\sqrt{(vt' - \rho\sin\psi)^2 + h^2 + \rho^2\cos^2\psi}}\, dt'. \quad (\ ^\cdot$$

As shown in Appendix B, the t' integral may be performed to give

$$\frac{\pi j}{v} H_o^{(1)}\left(k\sqrt{(h^2 + \rho^2\cos^2\psi)\left[1 - \left(\frac{\omega - \omega_o}{kv}\right)^2\right]}\right) \qquad (\ ^\cdot$$

where $H_o^{(1)}(z)$ is the zero order Hankel function of the first kind.

The integral in ω may be performed also for

$$H(\omega) = \frac{\sin\left[(\omega - \omega_o) \frac{T}{2}\right]}{(\omega - \omega_o) \frac{T}{2}}$$

(8

with the approximation $\left(\dfrac{\omega - \omega_o}{kv}\right)^2 <<< 1$ give

$$\left\{\begin{array}{ll} \dfrac{2\pi}{T} & ; \quad |t - \rho \sin \psi| \leq \dfrac{T}{2} \\[4mm] 0 & ; \quad |t - \rho \sin \psi| > \dfrac{T}{2} \end{array}\right\}$$

(8

With the substitution of Equations (80) and (82), Equation (79) becomes

$$S_y(t) = \frac{-k \exp (j\omega_o t)}{2vT} \int_o^{2\pi} d\psi \int_o^a \rho F(\rho) H_o^{(1)}\left[k \sqrt{(h^2 + \rho^2 \cos^2 \psi)}\right] d\rho$$

(8

for $|vt - \rho \sin \psi| < \dfrac{vT}{2}$, and

$$S_y(t) = 0$$

(8

for $|vt - \rho \sin \psi| > \dfrac{vT}{2}$. Equation (83) still contains a two-dimensional integral, but it has somewhat different properties from Equation (15): The

84

sampling function is not expressed explicitly, but appears implicitly in the limits, and the only approximation made in the evaluations is that

$$\left(\frac{\omega - \omega_o}{kv}\right)^2 <<< 1 \quad .$$

(8

This condition is met very well for typical system parameters, such as those discussed above.

That Equation (83) has basically the same character as Equation (15) may be seen by considering the asymptotic form of $H_o^{(1)}(z)$ for large values of the argument

$$H_o^{(1)}\left[k\sqrt{h^2 + \rho^2 \cos^2 \psi}\right] \longrightarrow \sqrt{\frac{2}{\pi}} \ \frac{\exp\left(jk\sqrt{h^2 + \rho^2 \cos^2 \psi}\right)}{\sqrt{k\sqrt{h^2 + \rho^2 \cos^2 \psi}}} \quad .$$

(86

With this substitution, the form of the two equations is identical ($\rho \cos \psi \equiv \xi$) with the exception of the $\frac{\sin u}{u}$ sampling function and an amplitude factor ($h^2 + \rho^2 \cos^2 \psi$ appears as the fourth root rather than the square root). However, as mentioned above, the sampling dependence is implicit in the limits of Equation (83).

APPENDIX B

To evaluate the integral

$$I_1 = \int_{-\infty}^{\infty} \frac{\exp\left\{-jk\left[\frac{\omega-\omega_o}{kv}(\rho \sin \psi - vt') + \sqrt{(\rho \sin \psi - vt')^2 + h^2 + \rho^2 \cos^2 \psi}\right]\right\}}{\sqrt{(\rho \sin \psi - vt')^2 + h^2 + \rho^2 \cos^2 \psi}} \, dt' \quad ,$$

the change of variable

$$x = -\frac{\rho \sin \psi - vt'}{\sqrt{h^2 + \rho^2 \cos^2 \psi}} + \frac{kv}{\omega - \omega_o}\sqrt{1 + \frac{(\rho \sin \psi - vt')^2}{h^2 + \rho^2 \cos^2 \psi}}$$

leads to a form with a more obvious solution.

$$I_1 = \int_{-\infty}^{\infty} \frac{\exp\left\{-j\frac{k\sqrt{h^2 + \rho^2 \cos^2 \psi}}{\frac{kv}{\omega - \omega_o}}x\right\}}{v\sqrt{1 - \left(\frac{kv}{\omega - \omega_o}\right)^2 + x^2}}$$

Now if the variable is changed once more to

$$y = \frac{x}{\sqrt{\left(\frac{kv}{\omega - \omega_o}\right)^2 - 1}} \quad ,$$

86

and the function

$$k \sqrt{(h^2 + \rho^2 \cos^2 \psi) \left[1 - \left(\frac{\omega - \omega_o}{kv}\right)^2\right]}$$

is designated by z, the familiar Bessel function integral is obtained

$$I_1 = \frac{1}{v} \int_{-\infty}^{\infty} \frac{\exp(-jzy)}{\sqrt{y^2 - 1}} \, dy \quad .$$

One way to solve this last integral is to separate the integral into two integrals over different parts of the region of integration.

$$I = \frac{1}{v} \int_{-\infty}^{\infty} \frac{\exp(-jzy)}{\sqrt{y^2 - 1}} \, dy = \frac{1}{v} \left\{ j \int_{-1}^{1} \frac{\exp(-jzy)}{\sqrt{1 - y^2}} \, dy + 2 \int_{1}^{\infty} \frac{\cos zy}{\sqrt{y^2 - 1}} \, dy \right\} \quad .$$

Now using the formulas from McLachlan[10]

$$\int_{-1}^{1} \frac{\exp(\pm jzy)}{\sqrt{1 - y^2}} \, dy = \pi J_o(z)$$

$$2 \int_{1}^{\infty} \frac{\cos zy}{\sqrt{y^2 - 1}} \, dy = -\pi Y_o(z) \quad ,$$

gives the relation

$$\mathbf{I}_1 = \frac{\pi j}{v} \left\{ J_o(z) + j Y_o(z) \right\} = \frac{\pi j}{v} H_o^{(1)}(z)$$

where $J_o(z)$, $Y_o(z)$, and $H_o^{(1)}(z)$ are the Bessel functions of zero order and argument z that are commonly designated by J, Y, and $H^{(1)}$. Reintroducing the value of z gives

$$\mathbf{I}_1 = \frac{\pi j}{v} H_o^{(1)} k \sqrt{\left[h^2 + \rho^2 \cos^2 \psi \right] \left[1 - \left(\frac{\omega - \omega_o}{kv} \right)^2 \right]} \quad .$$

REFERENCES

1. R. W. Bickmore. "On Focusing Electromagnetic Radiators", Canadian Journal of Physics, vol. 35 (November 1957), pp. 1292-1298.

2. D. K. Cheng. "On the Simulation of Fraunhofer Radiation Patterns in the Fresnel Region", IRE Transactions on Antennas and Propagation, vol. AP-5 (October 1957), pp. 399-402.

3. A. E. F. Grumpler. "AN/ASM-13 Airborne Antenna Pattern Recorder", 29 September 1960, Bendix Radio Division, Baltimore, Maryland.

4. S. Silver. Microwave Antenna Theory and Design, Volume 12 of MIT Radiation Laboratory Series, McGraw-Hill Book Co., Inc. (1959), p. 170.

5. H. H. Hougardy. "Scientific Report No. 1 - Transverse Doppler Pattern Measurement Technique", AFCRL-62-194 (62-ESD-9), Contract AF 19(604)-8362, 28 February 1962, American Systems Incorporated, Electromagnetic Systems Division, Hawthorne, California.

6. C. W. Sherwin, J. P. Ruina, and R. D. Rawcliffe. "Some Early Developments in Synthetic Aperture Radar Systems", IRE Transactions on Military Electronics, vol. MIL-6, No. 2 (April 1962).

7. H. L. McCord. "The Equivalence Among Three Approaches to Deriving Synthetic Array Patterns and Analyzing Processing Techniques", IRE Transactions on Military Electronics, vol. MIL-6, No. 2 (April 1962).

8. R. C. Spencer. "Fourier Integral Methods of Pattern Analysis", Report No. 762-1, 21 January 1946, Massachusetts Institute of Technology, Radiation Laboratories.

9. W. E. Gordon and L. M. LaLonde. "The Design and Capabilities of an Ionospheric Radar Probe", IRE Transactions on Antennas and Propagation, vol. AP-9 (January 1961), pp. 17-22.

REFERENCES (Continued)

10. N. W. McLachlan. **Bessel Functions for Engineers**, Oxford University Press, London (1955), p. 192 (No. 43) and p. 197 (No. 116).

BIBLIOGRAPHY

1. R. B. Barrar and C. H. Wilcox. "On the Fresnel Approximation", IRE Transactions on Antennas and Propagation, vol. AP-6 (January 1958), pp. 43-48.

2. Dr. R. W. Bickmore. "Fraunhofer Pattern Measurement in the Fresnel Region", Canadian Journal of Physics, vol. 35 (November 1957), pp. 1299-1308.

3. Dr. R. W. Bickmore and Dr. R. C. Hansen. "Antenna Power Densities in the Fresnel Region", Proceedings of the IRE, vol. 47 (December 1959), pp. 2119-2120.

4. R. F. Goodrich and R. E. Hiatt. "On Near Zone Antennas", Final Report 2861-1-F, June 1959, University of Michigan.

5. M. Handelsman. "Technical Note on Focusing Properties of a Linear Antenna with a Spherical Phase Front", October 1958, Rome Air Development Center, Griffiss Air Force Base, DCS/ Operations.

6. Dr. R. C. Hansen and L. L. Bailin. "Near Field Analysis of Circular Aperture Antennas", Scientific Report No. 3, Contract AF 19(604)-3508, August 1959, Hughes Aircraft Company, Systems Development Laboratory, Culver City, California.

7. Dr. R. C. Hansen, L. L. Bailin, and R. W. Rutishauser. "On Computing Radiation Integrals", Comm. Assoc. Computing Machinery, vol. 2 (February 1959), pp. 28-31.

8. M. K. Hu. "Study of Near Zone Fields of Large Aperture Antennas", Final Report, RADC-TR-57-126A and B, Contract AF 30(602)-928, April 1957, Syracuse University, Research Institute, Syracuse, New York.

9. A. F. Kay. "Far Field Data at Close Distances", Contract AF 19(604)-1126, October 1956, Technical Research Group, Inc., New York, New York.

10. A. F. Kay. "Near Field Gain", Report No. SR 131-1, Contract AF 19(604)-5532, August 1959, Technical Research Group, Inc., New York, New York.

BIBLIOGRAPHY (Continued)

11. Little. "Gain Measurements of Large Aerials Used in Intefe-rometer and Cross-Type Radio Telescopes", _Australian Journal of Physics_ (1958), pp. 70-78.

12. J. H. Richmond. "A Modulated Scattering Technique for Meas-urement of Field Distributions", _IRE Transactions on Microwave Theory and Techniques_, vol. MTT-3 (July 1955), pp. 13-15.

13. A. T. Villeneuve. "Antenna Research: Part VI - Near Zone Pattern Synthesis by the Focusing Method", Final Report, September 1959, Syracuse University, Research Institute.

UNCLASSIFIED

1. Antenna Radiation
   Patterns--Analysis
2. Antenna Radiation
   Patterns--Measurement

I. Hougardy, H. H.
II. McFadden, R. K.
III. Air Force Cambridge
   Research Laboratories,
   Electronic Research
   Directorate, Bedford,
   Massachusetts
IV. Contract AF19(604)-8362

UNCLASSIFIED

AD-

Teledyne Systems Corporation, Electromagnetic Systems Division, Hawthorne, California.
TRANSVERSE DOPPLER PATTERN MEASUREMENT TECHNIQUE, by H. H. Hougardy and R. K. McFadden. 1 February 1963. 92p. incl. illus. tables, 11 refs. (Project 4600; Task 46007) (Final Report No. 63-ESD-18; AFCRL-63-94) Unclassified Report
(Contract AF 19(604)-8362)

This report contains the results of an analytic investigation of the Transverse Doppler Pattern Measurement Technique for determining the far field radiation characteristics of large antennas from near field measurements. The technique is based on using Doppler signal processing to obtain the information necessary for predicting the far field patterns of large antennas in their site environments. Primary emphasis has been placed on establishing a rigorous mathematical description of

(over)

UNCLASSIFIED

AD-

the measurement process from which system parameters and performance may be determined.

Several mathematical models have been developed which differ both in the analytical approach and in the physical make-up of the measuring system. Mathematical approximations for the diffraction field of the aperture have been expanded in several coordinate frames. The signal processing systems investigated include multi-channel processing, synthetic aperture processing, and directional and nondirectional sampling antennas. Attention has been given to linear arrays, rectangular arrays with separable and nonseparable distributions, circular apertures with circularly symmetric distribution, and arbitrarily shaped radiating apertures with large linear phase deviations. Two experimental procedures have been outlined for the purpose of verifying the feasibility of the analytical work.

UNCLASSIFIED

UNCLASSIFIED

1. Antenna Radiation
   Patterns--Analysis
2. Antenna Radiation
   Patterns--Measurement

I. Hougardy, H. H.
II. McFadden, R. K.
III. Air Force Cambridge
   Research Laboratories,
   Electronic Research
   Directorate, Bedford,
   Massachusetts
IV. Contract AF19(604)-8362

UNCLASSIFIED

AD-

Teledyne Systems Corporation, Electromagnetic Systems Division, Hawthorne, California.
TRANSVERSE DOPPLER PATTERN MEASUREMENT TECHNIQUE, by H. H. Hougardy and R. K. McFadden. 1 February 1963. 92p. incl. illus. tables, 11 refs. (Project 4600; Task 46007) (Final Report No. 63-ESD-18; AFCRL-63-94) Unclassified Report
(Contract AF 19(604)-8362)

This report contains the results of an analytic investigation of the Transverse Doppler Pattern Measurement Technique for determining the far field radiation characteristics of large antennas from near field measurements. The technique is based on using Doppler signal processing to obtain the information necessary for predicting the far field patterns of large antennas in their site environments. Primary emphasis has been placed on establishing a rigorous mathematical description of

(over)

UNCLASSIFIED

AD-

the measurement process from which system parameters and performance may be determined.

Several mathematical models have been developed which differ both in the analytical approach and in the physical make-up of the measuring system. Mathematical approximations for the diffraction field of the aperture have been expanded in several coordinate frames. The signal processing systems investigated include multi-channel processing, synthetic aperture processing, and directional and nondirectional sampling antennas. Attention has been given to linear arrays, rectangular arrays with separable and nonseparable distributions, circular apertures with circularly symmetric distribution, and arbitrarily shaped radiating apertures with large linear phase deviations. Two experimental procedures have been outlined for the purpose of verifying the feasibility of the analytical work.

UNCLASSIFIED